

The Faculty of Suleyman Sami Nalbant Is Approved:

MINE  
LIBRARY  
THESIS  
2890

*David A. Mouat*  
Thesis Advisor  
Mackay School of Mines  
University of Nevada - Reno

✓ *4477*  
Lithologic and Structural Analysis of A Part of Western  
Turkey By Using Landsat TM Data

*Suleyman Sami Nalbant*  
M.S. Candidate  
Mackay School of Mines

A thesis submitted in partial fulfillment of the  
requirements for the degree of Master of Science in  
Geophysics

APPROVED BY FACULTY

by

Suleyman Sami Nalbant

IN

David A. Mouat/Thesis Advisor

December 1991

December 1991

The thesis of Suleyman Sami Nalbant is Approved:

*David L. Mauat*

\_\_\_\_\_  
Thesis Advisor

*M. W. W. W.*

\_\_\_\_\_  
Department Chair

*Ronald C. Dillaway*

\_\_\_\_\_  
Dean, Graduate School

University of Nevada

Reno

December 1991

**ACKNOWLEDGMENTS**

I would like to gratefully thank my adviser, Dr. David A. Mouat for his support and assistance. Through his efforts, I was able to use the VAX 11/780 IDIMS image processing facility.

Appreciation is extended to my committee members, Prof. Lawrence T. Larson, Dr. Robert J. Watters, and Dr. Yunus A. Cengel for their advice and manuscript review and criticism. Special mention is rendered to Prof. Larson who generously provided Landsat TM data, geologic information and shared his experiences about the study area, and Dr. Cengel who supported and helped me about every problem I had, since I came Reno.

I am also grateful to the System Manager, James Granata for his positive attitude and training me in application of imagery processing on the School's IDIMS system. I am pleased to recognize Charles Sabine, fellow Ph. D. student for helpful discussions and suggestions. I thank Zhongmin Yu for his kind helps.

This work was supported by the Ministry of Education of Turkey, and partially supported by a scholarship-loan from the Women's Auxiliary to the American Institute of Mining, Metallurgical and Petroleum Engineers, Inc. (WAAIME). I am grateful for their support.

Lastly, I would like to thank my wife, Zehra Nalbant, for her support and patience during the last one year.

**ABSTRACT**

The Korucu-Dugla study area (225 km<sup>2</sup>) located within western Turkey was selected for application of Landsat Thematic Mapper (TM) data to geological studies. A wide variety of image processing techniques including principal component analysis (PC), selective principal component analysis (SPC), decorrelation stretching (DS), intensity-saturation-hue transformation (ISH), TM band ratios, and edge enhancement were applied to discriminate the lithologies and structure as well as associated areas of hydrothermal alteration.

Color composites of PC1,PC2,PC3, always encoded red, green, blue respectively, PC4,PC3,PC2, DS4,DS5,DS6, and TM bands 5,4,1 were found most suitable for lithology and boundary discrimination in the area. SPC4 of TM bands 1,3,4,5 and SPC4 of TM bands 1,3,5,7 were accomplished for mapping iron-oxide and hydroxyl-bearing areas respectively. The use of both SPC images is the best technique to separate hydrothermally altered areas. Hydrothermally altered areas, which have potential for mineralization, were mapped on the constructed geologic map. A number of previously unmapped faults and subunits of the formations were discriminated successfully.

A lineament map and rose diagram were prepared using high-pass Laplacian filters. The rose diagram showed a good correspondence with previously mapped earthquake strike and

breaks. The linear features of the area have dominant directions at N. 30-40° E. and N 60-80° E. Alteration and mineralization in the Korucu-Dugla area are mostly controlled by NNE- and EW-trending structures.

Study Area and Climate.....	4
CHAPTER II. GEOLOGY OF THE STUDY SITE.....	5
Geologic Setting.....	7
Hydrothermal Alteration in the Study Area.....	12
Previous Geological Work .....	14
Geologic Formations.....	21
Permian Rocks.....	21
Triassic Rocks.....	21
Tertiary Rocks .....	22
CHAPTER III. METHODOLOGY.....	28
The Mission and Rationale For The Data.....	28
Atmospheric Correction.....	28
Imagery Analysis.....	28
Field Investigation .....	33
Laboratory Spectra Measurements.....	35
CHAPTER IV. SPECTRAL CHARACTERIZATION.....	35
Basic Spectral Characteristics of Rocks.....	35
Spectral Characteristics of Formations in the Study Area.....	38
CHAPTER V. IMAGERY ANALYSIS AND RESULTS .....	50
Single Band Images.....	50

TABLE OF CONTENTS

	Page
<b>CHAPTER I. INTRODUCTION</b> .....	<b>1</b>
Statement of Problem.....	1
Study Area and Climate.....	4
<b>CHAPTER II. GEOLOGY OF THE STUDY SITE</b> .....	<b>7</b>
Geologic Setting.....	7
Hydrothermal Alteration in the Study Area.....	12
Previous Geological Work .....	14
Geologic Formations.....	21
Permian Rocks.....	21
Triassic Rocks.....	21
Tertiary Rocks .....	22
<b>CHAPTER III. METHODOLOGY</b> .....	<b>25</b>
TM Mission and Rationale For TM Data.....	25
Atmospheric Correction.....	26
Imagery Analysis.....	28
Field Investigation .....	33
Laboratory Spectra Measurements.....	33
<b>CHAPTER IV. SPECTRAL CHARACTERISTICS</b> .....	<b>35</b>
Basic Spectral Characteristics of Rocks.....	35
Spectral Characteristic of Formations in the Study Area.....	38
<b>CHAPTER V. IMAGERY ANALYSIS AND RESULTS</b> .....	<b>50</b>
Single Band Images.....	50

Single Band Composites.....	55
2-1-1 Ratios.....	58
2-1-2 Principal Components Analysis.....	61
2-1-3 Decorrelation Stretching.....	65
Selective Principal Components Analysis.....	67
ISH Transformation.....	73
2-1-4 Complex Composite Images.....	75
2-2-1 Directional Filtering and	
Structural Map of the Area .....	77
<b>CHAPTER V. CONCLUSIONS.....</b>	<b>85</b>
<b>REFERENCES.....</b>	<b>90</b>
<b>APPENDIX A.....</b>	<b>96</b>
<b>APPENDIX B.....</b>	<b>99</b>
3-1-1 a) Color composite of VN bands 3, 2 and 1 (in RGB) before atmospheric correction, b) after atmospheric correction. Note bluish haze in (a)...	51
3-1-2 Location of sample sites in the study area.....	71
4-1-1 Features due to electronic transitions in the spectra of iron-bearing minerals. Spectra are displayed vertically, and characteristic features are indicated by arrows (after Hunt and Ashley, 1978).....	37
4-1-2 Selected laboratory spectra of minerals containing quartz vibrational absorption features for Al-OH (2.16 to 2.22 $\mu$ m), Mg-OH (2.3 to 2.36 $\mu$ m), and CO <sub>2</sub> (2.3 to 2.36 $\mu$ m). VN band 3 is indicated (after Goetz, Yano, Solomon and Rock, 1985).....	31
4-2-1 Surface laboratory spectra of samples	

## LIST OF FIGURES

Figure	Page
1-1. Location map of the study area.....	2
1-2. Normal color composite of TM bands 3, 2, and 1 (in RGB), and some towns in the study area. Vegetated areas are shown in dark color. Formations in the area can not be separated.....	5
2-1. Geologic map of the study area and surrounding region (modified from Akyurek and Soysal, 1981)...	8
2-2. Geologic map of the study area (modified from Akyurek and Soysal, 1981).....	10
2-3. Geologic map of a part of the study area (modified from Mariko, 1970).....	15
2-4. Geologic map of a part of the study area (modified from Ozcan, 1972).....	16
2-5. Recent tectonic structure of Turkey and geothermal areas (after Larson, 1989).....	18
3-1. a) Uncorrected Landsat TM digital numbers (DNs) for bands 1, 2, 3, 4, 5, and 7 plotted at band center wavelengths for two agricultural areas ("veg. sites"). b) corrected DN's for the same sites. Note, especially the removal of haze in the shorter wavelength region.....	30
3-2. a) Color composite of TM bands 3, 2 and 1 (in RGB) before atmospheric correction, b) after atmospheric correction. Note bluish haze in (a)...	31
3-3. Location of sample sites in the study area.....	34
4-1. Features due to electronic transitions in the spectra of iron-bearing minerals. Spectra are displaced vertically, and characteristic features are indicated by arrows (after Hunt and Ashley, 1979).....	37
4-2. Selected laboratory spectra of minerals containing overtone vibrational absorption features for Al-OH (2.16 to 2.22 $\mu\text{m}$ ), Mg-OH (2.3 to 2.35 $\mu\text{m}$ ), and CO (2.3 to 2.35 $\mu\text{m}$ ). TM band 7 is indicated (after Goetz, Vane, Solomon and Rock, 1985).....	37
4-3. Beckman laboratory spectra of samples	



from sample sites 20 and 21 from the Kinik Formation. Note clear carbonate absorption near 2.35 $\mu\text{m}$ .....	39
4-4. Published laboratory spectra of a variety of sandstones (a), and limestones (b). The spectra are displaced vertically, and percent reflectance markers are separated by 10 % (from Hunt and Salisbury, 1976).....	41
4-5. A chosen laboratory spectrum of a sample (a clay-carbonate rich sediment) from sample site 15, from the Soma Formation. Note clay and carbonate absorptions near 2200 and 2350 respectively.....	42
4-6. Laboratory spectrum (Beckman) of the Caldag Limestone Member. Note similar spectral characteristics with Figure 4-4b.....	42
4-7. Published laboratory spectra of green schist (a), and chlorite schist (b) (modified from Hunt and Salisbury, 1976).....	44
4-8. Reflectance curves for vegetation, unaltered rocks, and hydrothermally altered rocks (from Sabins, 1987).....	44
4-9a. Laboratory spectrum of unaltered andesite from sample site 2 from the Yunutdag Volcanics. Compare with fresh andesite spectrum (4-9b).....	45
4-9b. Published Beckman laboratory spectrum of fresh andesite (from Collins, 1988).....	46
4-10. Laboratory spectra of samples from sample sites 4, 5, and 6 in the Yunutdag Volcanics. Alteration types indicated on spectra.....	47
4-11. Beckman laboratory spectrum of perlite (sample number is 7). Note the clay absorption feature around 2.2 $\mu\text{m}$ .....	48
4-12. Published laboratory spectra of granite (from Sultan et al., 1987).....	49
5-1. Atmospherically corrected and stretched (Gaussian type) TM band 1 (a), band 2 (b), band 3 (c), band 4 (d), band 5 (e), and band 7 (f).....	52
5-2. TM band 5, 4, and 1 (in RGB) composite of the study area (512 x 512 pixels). Note distinctive purple over the Kinik and the Caldag Formations due to their relatively high reflectance spectra	

in band 5 and 1.....	56
5-3. TM bands 4, 3, and 2 false color image. Note the red hues over vegetated areas due to their high reflectance in band 4 relative to bands 3 and 2...	57
5-4. TM color composite of ratio images 3/1, 4/3 and 5/7 (in RGB). Altered areas in Yunutdag volcanics and andesites appear magenta and are marked by arrows. The magenta areas within the Soma Formation are due to the concentration of clay and carbonate minerals in this formation.....	60
5-5. Color composite image of principal components PC1, PC2, PC3.....	63
5-6. Color composite of principal components PC4, PC3, and PC2.....	64
5-7. Color composite image of decorrelation components DS4, DS5, and DS6. Dark magenta and pink represent vegetated areas. Altered areas are in distinctive light green.....	66
5-8. SPC4 shows iron-oxide bearing areas as bright pixels. Note the areas indicated by arrows.....	71
5-9. Negated SPC4 of TM bands 1, 4, 5 and 7 which shows hydroxyl bearing areas as bright pixels. Note the areas indicated by arrows.....	72
5-10. ISH transformed image of TM bands 1, 3 and 5. Intensity=red, saturation=green, hue=blue. Dacites are in purple hues, andesites are in dark magenta and dark red. Note red areas over the Kinik Formation (7C,10C).....	74
5-11. Color composite image of SPC4 of TM 1,4,5,7, PC4, and SPC4 of TM 1,3,4,5 (in RGB).....	76
5-12. Directional filter kernel (from Sabins, 1988).....	77
5-13. Lineament map of the study area which is constructed from directionally filtered images....	78
5-14. Rose diagram of lineaments identified on Landsat TM image in the study area. n = number of lineaments.....	80
5-15. Slip vectors and surface breaks of historical and recent earthquakes in western Turkey, and the rose diagram of lineaments in the study area.	

Note the good correlation between the rose diagram and the slip vectors (modified from McKenzie, 1978)..... 81

5-16. Geologic and structural map constructed from the color composites, field work of the author, and works of Akyurek and Soysal (1981), Ozcan (1972), and Mariko (1970)..... 83

#### LIST OF TABLES

Table	Page
1. Generalized stratigraphic section of the Korucu Bergama Province (from Akyurek and Soysal (1981), Ercan et al. (1984)).....	19
2. Landsat 5 Thematic Mapper images and image composites analyzed at the study area. All composite images are color encoded in red, green, and blue (RGB).....	32
3. Geological features discriminated in Thematic Mapper bands 1, 2, 3, 4, 5, and 7.....	51
4. Selected principal component analysis for iron-oxide mapping.....	68
5. Selected principal component analysis for hydroxyl mapping.....	69

## CHAPTER I

### INTRODUCTION

#### STATEMENT OF PROBLEM

The use of satellite images for geological mapping and for exploring economic resources is becoming increasingly important. After the launch of the Thematic Mapper (TM) sensor on Landsat 4 in 1982, geologists had access to better spatial (30 m) and spectral resolution, compared to the multispectral scanner (MSS), for detailed geologic studies. Many geologic studies have employed TM data to discriminate the various lithologies associated with hydrothermal alteration. Geologic mapping in many parts of the world (including Turkey) has only been superficial, in part because of access, and in part because of vegetation cover.

The Korucu-Dugla study area (225 km<sup>2</sup>) of western Turkey was selected for application of Landsat TM imagery to geological studies (Figure 1-1) because the area has a variety of lithologies that are of interest to geologists. The purpose of this study is to use spaceborne remote sensing as a tool to examine lithology, structure, and hydrothermal alteration in the Korucu-Dugla Province as well as to answer the following questions:

1. Can TM data be used for lithologic mapping for areas having considerable vegetation cover?



Figure 1-1. Location map of the study area.

2. Can meaningful structural relationships be interpreted from lineament analyses derived from the remote sensing imagery?
3. Is it possible to discriminate hydrothermally altered areas with remote sensing in an area of varied lithologies having a moderate vegetation cover?
4. Is there any relationship between the known ore deposits of the study area and lineaments?
5. What is the most suitable type of TM image processing for lithologic discrimination of the study area?

The study area is one of the few areas of Turkey which has published geologic maps at a scale of 1:100,000 or larger. Another reason for choosing this area is its potential of precious metal mineralization. Recently, to the southwest of the study area, around the town of Dikili, very close to Bergama (Figure 1-1), gold mineralization was found. In addition, the study area includes a number of antimony, lead-zinc and copper prospects associated with hydrothermal activity (M.T.A., 1970; Ozcan, 1972; Mariko, 1970).

The east side of the study area is covered by Triassic volcanics that are part of west Anatolia's volcanic belt. The

known gold mineralization at Arapdagi, Izmir, is located at the southern end of this volcanic belt (Figure 1-1). Gold mineralization at Arapdagi is hosted by hydrothermally altered Tertiary dacitic tuffs (Sayili et al., 1990).

#### STUDY AREA AND CLIMATE

The study area consists of a region of approximately 15 km x 15 km in size, and lies mainly north of the Aegean Region in western Turkey, some 30 km southwest of the city of Balikesir (Figure 1-1). Towns within the area are Korucu, Buyukyenice, Tasdibi, Dugla, Cicekli as well as a number of very small villages (Figure 1-2).

An asphalt road connects the towns of Dugla, Tasdibi, Buyukyenice and Korucu. The other villages are connected by gravel roads which can be useless after heavy rain.

The Korucu Mountains border the west of the study area from north to south. A part of the Turkali Mountains, which trend east-west, occurs in the east side of the study area. The Koca River is the principal river in the area. There are two main branches of the Koca river, one of which flows from south to north at the west side of the area. The other branch lies between the Koca Mountains and the Turkali Mountains in the middle of the area. These branches join together at the north of the study area.

Elevations in the study area range from 300 m at Koca River to 816 m at Asar Hill, Koca Mountains.

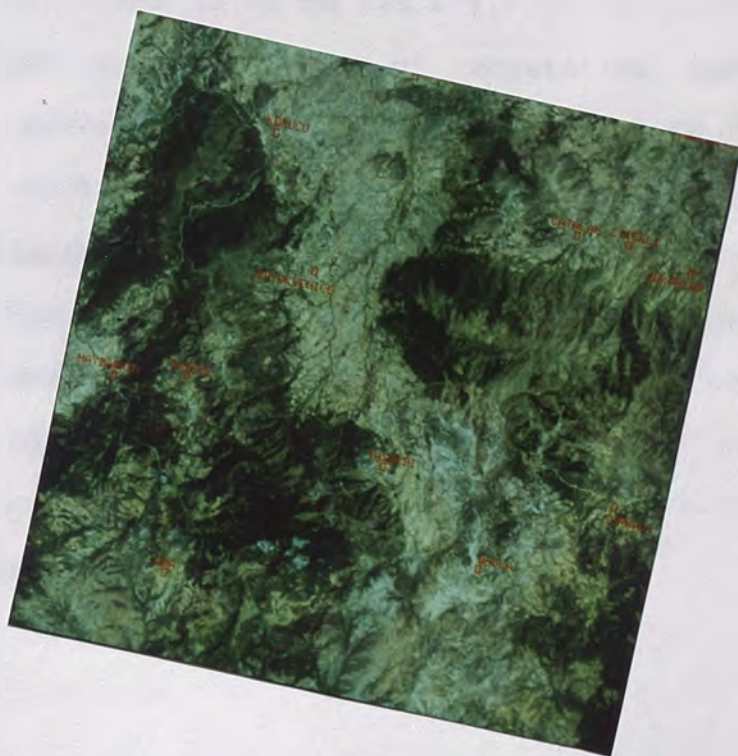


**Figure 1-2.** Normal color composite of TM bands 3, 2, and 1 (in RGB), and some towns in the study area. Vegetated areas are shown in dark color. Formations in the area can not be separable.



The climate of the area is semi-arid, with warm summers and cold winters. The annual average temperature is 14.6°C (58°F), and the highest recorded temperature is 41°C (106°F). In winter, temperatures may drop to as low as -7.6°C (19°F). Precipitation occurs most often in the winter months with the summers typically dry. The highest precipitation is recorded in December, and the lowest is recorded in August. Average annual precipitation is 65 cm (25.5").

The type and abundance of vegetation varies with elevation. Areas up to 300-400 m are covered by scrub type vegetation, such as Quercus ilex, Quercus aegilops, Arbutus unedo and Olea spp. Areas over 500 m are typically covered by pines with Pinus ibrutia and Pinus nigra predominating. In the valley sections of the study area there are some cystus and barley (Hordeum vulgare) fields. Along the rivers and streams grow several species of poplar (Populus spp.) and willow (Salix spp.).

The recent period of volcanic activity resulted in widespread andesite, dacite, trachyandesite, rhyolitic lavas, tuffs and silicified tuffs (Boris et al., 1984). These volcanics were named "Jumisdag Volcanics" by Akyuzel and Soyual (1981) (Figure 1-1 and Figure 2-3). Tuffs crop out over large areas, and lava flows form smaller features. Most of the lavas are silicified, argillized, and pyritized (Boris et al., 1984; Erler and Larson, 1980). Krashinsky (1978) indicated high copper-silver concentrations in the volcanics, and a direct relationship between the concentration and

## CHAPTER II

### GEOLOGY OF THE STUDY SITE

#### GEOLOGIC SETTING

Most of the study area is covered by Tertiary lacustrine sediments, volcanics, metavolcanics and metasediments. The oldest exposed rock in the area is Permian allochthonous limestone blocks which is distributed on metasediments and metavolcanics (Kinik Formation).

The study area and surrounding region were affected by volcanic activity three times during the Tertiary (Erçan et al., 1984). The first period of volcanism resulted in andesitic-dacitic volcanics which can be seen in out crops approximately 10 km north of the study area. These volcanics were named the "Bagburun Formation" by Krushensky (1976). Later Eocene age plutonism emplaced the Kozak granodiorite to the north of the town of Bergama (Figure 2-1).

The second period of volcanic activity resulted in widespread andesite, dacite, trachyandesite, rhyodacitic lavas, tuffs and silicified tuffs (Erçan et al., 1984). These volcanics were named "Yunutdag Volcanics" by Akyurek and Soysal (1981) (Figure 2-1 and Figure 2-2). Tuffs crop out over large areas, and lava domes form smaller features. Most of the lavas are silicified, argillized, and pyritized (Erçan et al., 1984, Erler and Larson, 1990). Krushensky (1976) indicated high copper-zinc concentration in the volcanics, and a direct relationship between the concentration and

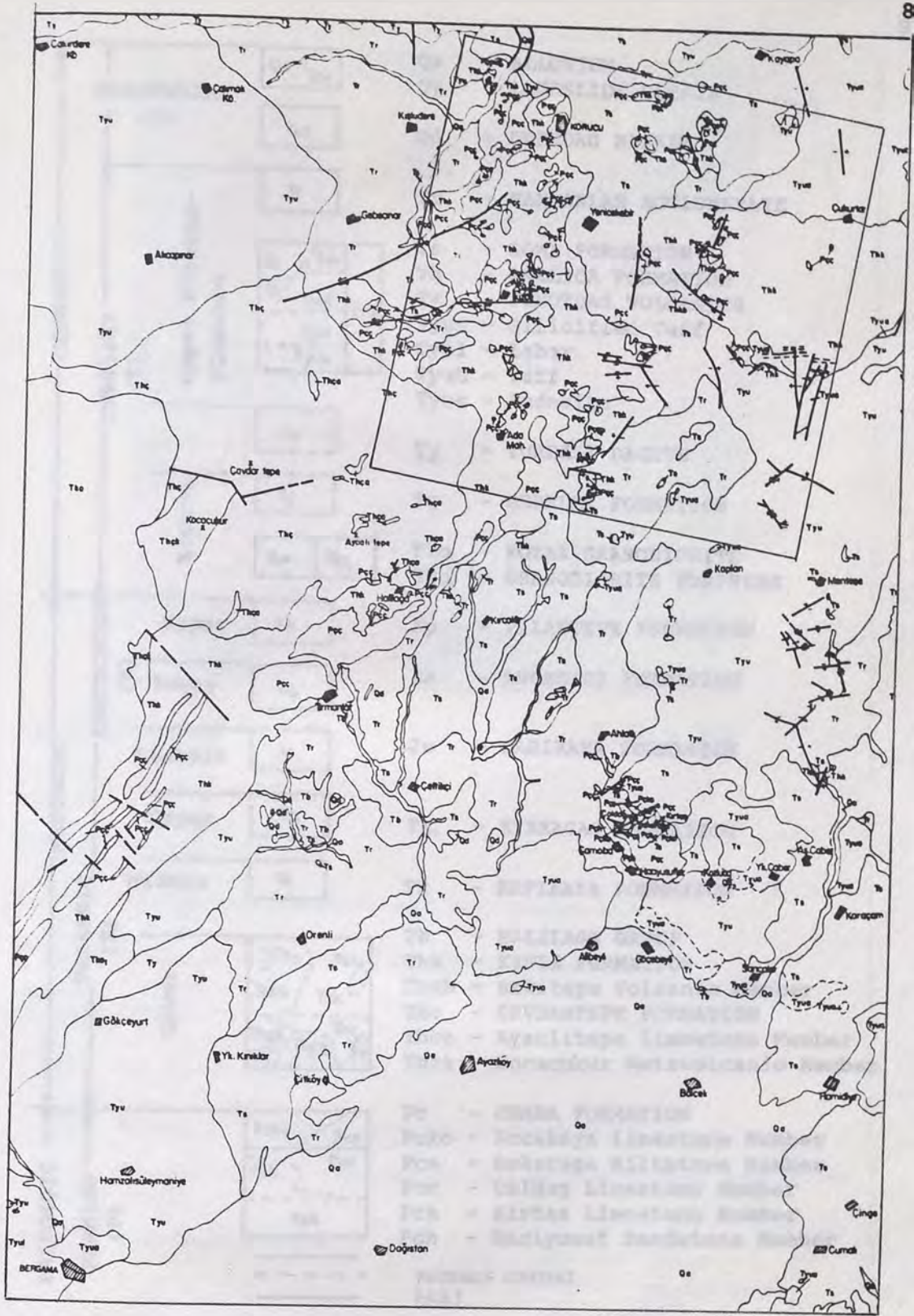


Figure 2-1. Geologic map of the study area and surrounding region (modified from Akyurek and Soysal, 1981).

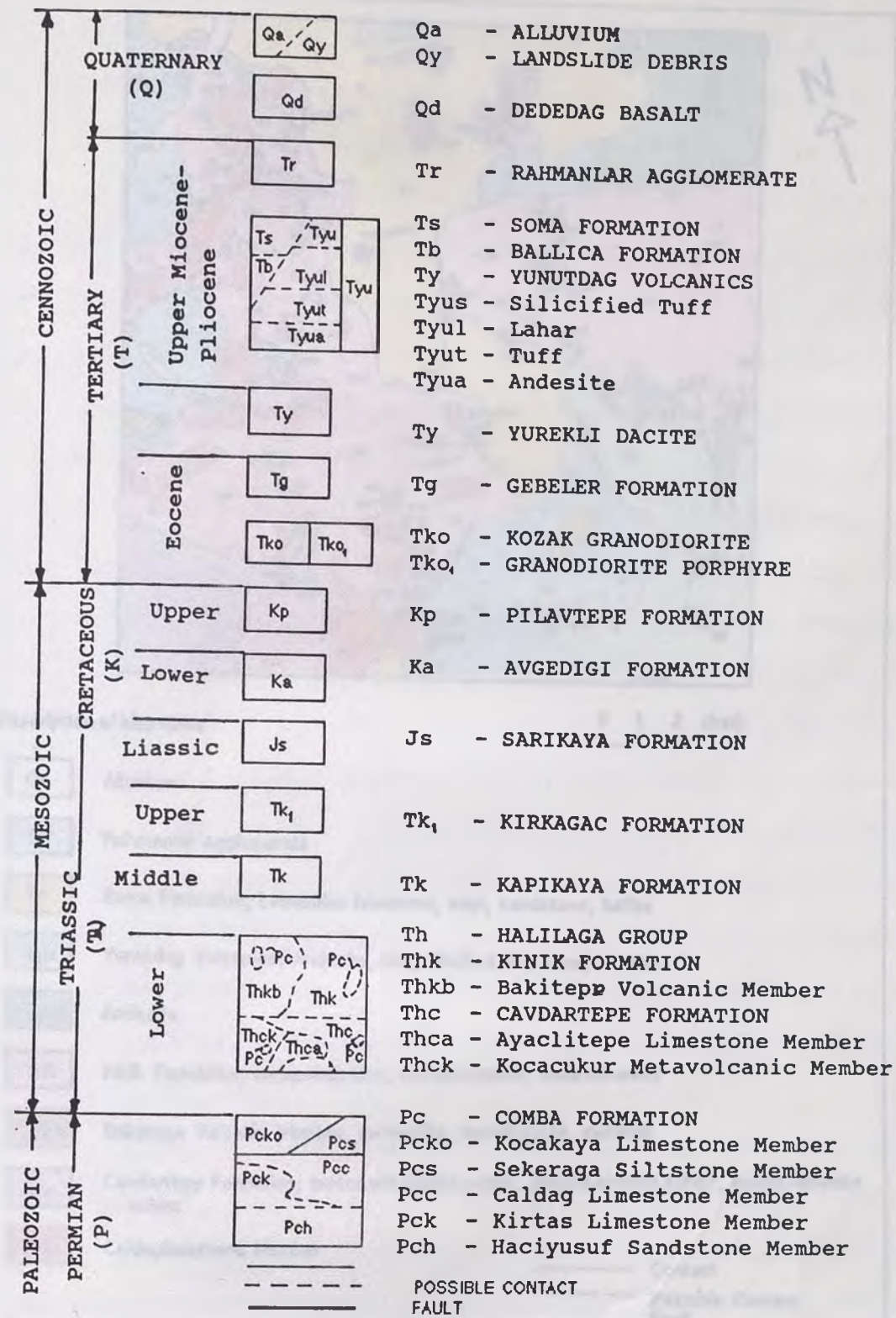


Figure 2-1. (continued) Geologic map of study area and surrounding region (modified from Akyurek and Soysal, 1981).

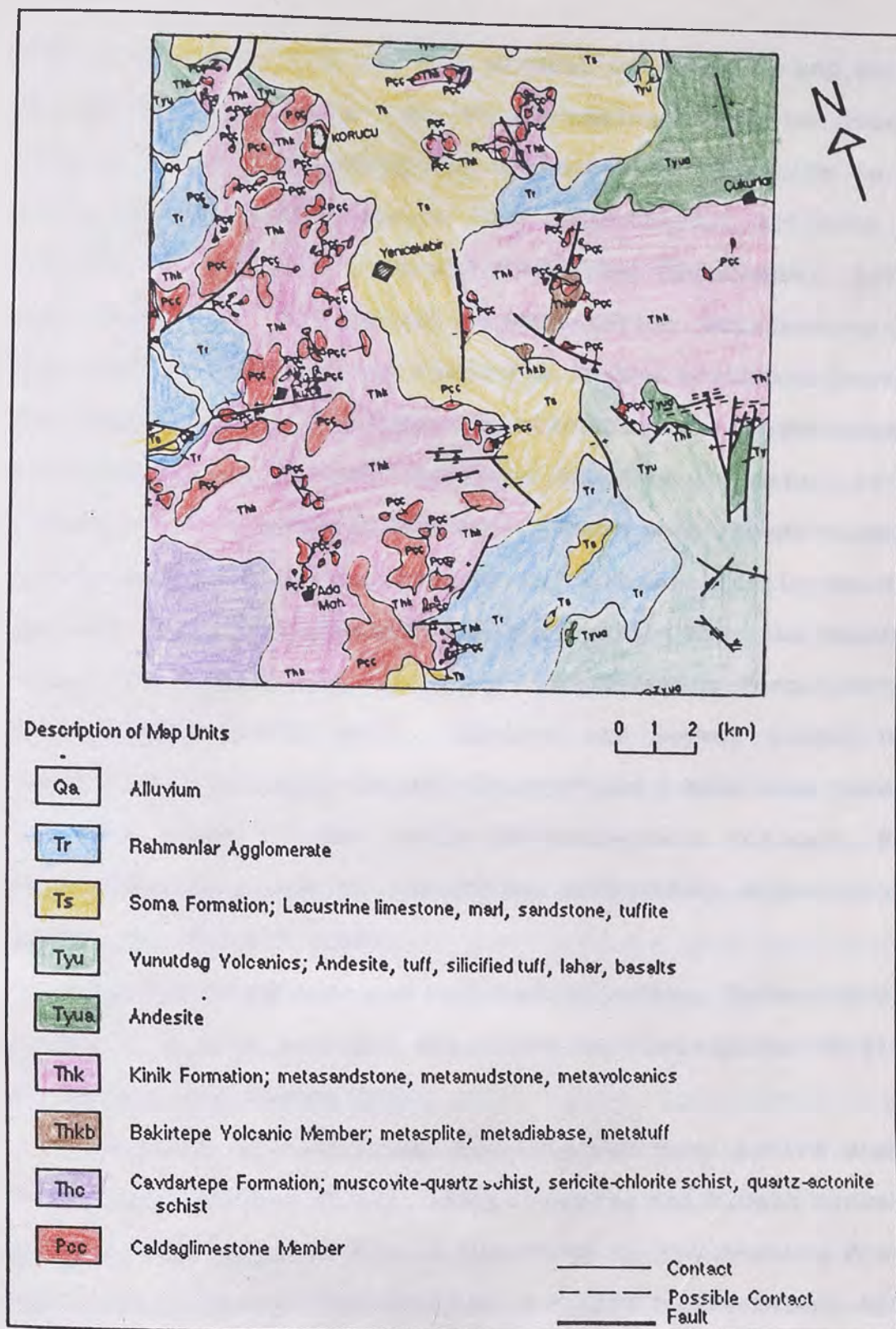


Figure 2-2. Geologic map of the study area (modified from Akyurek and Soysal, 1981).

alterations. In general, the mineral content (Cu and Pb-Zn) of volcanics increases with increasing alteration (Ozcan, 1972). The well-crystallized character of kaolinite in the volcanics strongly suggests that hydrothermal activity was responsible for the widespread alteration (Krushensky, 1976). Some lead-zinc and copper mineralization occurrences are reported in the Yunutdag volcanics in the southeast part of the study area. The Yunutdag volcanics are unconformably overlaid by the younger volcanics that are the result of the third period of volcanic activity. These more recent volcanic rocks consist of dacite, rhyodacite, and rhyolite in the form of lava flows and tuffs that are more acidic than the Yunutdag volcanics. This unit is called the "Dedetepe Formation" in Krushensky's (1976) work. Akyurek and Soysal (1981) have named these volcanics "Yurekli Dacite" and I have used Yurekli in this study. The Middle Miocene-Lower Pliocene Soma Formation, composed of lacustrine sediments, unconformably covers the Yurekli Dacite.

For the study area and surrounding region, Korucu-Bergama province, a more detailed stratigraphic description is given in Table 1 and Figure 2-1.

In terms of tectonism, Anatolia was very active during the Neogene (Sengor et al., 1985). During the Middle Miocene, Anatolia was squeezed toward the north by the Arabian Plate. North and northwest directions were sealed by the stable Asian Platform, and the east was also closed by Southern Russia and Iran. Therefore, only westward extension was possible, and

Anatolia moved westward. As a result of this movement, a number of horst-graben structures (11) were formed in west Anatolia (Turkey) (Figure 2-5).

#### HYDROTHERMAL ALTERATION IN THE STUDY AREA

Alteration caused by hydrothermal water by reaction with pre-existing solid phases is called hydrothermal alteration (Bates and Jackson, 1987). Ore minerals are deposited from hydrothermal solutions which also interact chemically with the country rock to alter the mineral composition for considerable distances beyond the site of ore deposition. The hydrothermally altered country rocks contain distinctive assemblages of secondary, or alteration, minerals that replace the original rock constituents. Alteration minerals commonly (not entirely) occur in distinct zones of hydrothermal alteration, relative to the ore body. These zones are caused by changes in temperature, pressure, and chemistry of the hydrothermal solution at progressively greater distance from the ore body (Sabins, 1987). At the time of ore deposition, the zones of altered country rock may not extend to the surface of the ground. Later uplift and erosion expose successively deeper alteration zones and eventually the ore body itself (Guilbert and Park, 1986). Not all alteration is associated with ore bodies, and not all ore bodies are marked by alteration zones, but these zones are valuable indicators of possible deposits. More information about hydrothermal alteration, zones of hydrothermal alteration and weathering processes are given in

the Appendix B. Mineralization and alteration in the study area are related to hydrothermal activity (Ozcan, 1972; Ercan et al., 1984; Erler and Larson, 1990). Lead-zinc and copper mineralization on Ozcan's (1972) map (Figure 2-4) were described as hydrothermal. In addition, argillic, montmorillonitic and sericitic alteration types are identified by laboratory spectra measurements on samples from sample sites 5, 4 and 6 respectively. These sample sites are very close to the locations of mineralization shown by Ozcan (1972).

A disseminated type stibnite deposit near Tasdibi village was described by M.T.A. (1970). Ore occurs along the contact between andesites and a large silica dike, which is at least 50 m wide and strongly brecciated in this deposit. Idiomorphic stibnite is concentrated in clusters along this contact. The andesites are completely argillized. Within the alteration zone the dominant mineral is kaolinite.

Jancovic (1982) studied the Gumuskoy deposit, Kutahya, west Turkey, a Sb-As-Tl-Ba mineral assemblage and speculated about other stibnite deposits in Western Anatolia. These deposits, including stibnite deposits in the study area, have been deposited mostly from highly differentiated hydrothermal solutions, and genetically related with the Neogene volcanics and granodiorite magma. He also pointed out an association of Pb-Zn sulphides, and minor amounts of silver and gold to the Gumuskoy mineral assemblage.

Although alteration in the study area is mostly related



hydrothermal solutions, outcropping kaolinite, montmorillonite and sericite can be produced by weathering processes. Therefore, areas mapped as possible hydrothermally altered areas in the Chapter V should be checked in the field.

The spectral characteristic of same hydrothermally altered minerals are discussed in Chapter IV.

#### PREVIOUS GEOLOGIC WORK

The first geologic study in the area was by Burkut (1966) who made a comparative genetic analysis of plutons in northwest Anatolia. Izdar (1968) studied the petrology and origin of volcanic rocks around the Kozak intrusive. Mariko (1970) mapped the geology at a scale of 1:10,000 of the area between Buyukyenice and Tasdibi inside the study area (Figure 2-3). Figure 2-3 is simplified from his study and is used as a secondary reference map in this study. Ozcan (1972) reported on the mineral potential of the area between Cicekli and Turkali (Figure 2-4) in the eastern part of the study area. He mapped some copper and lead-zinc occurrences in the area and estimated them as uneconomic reserves. His map is also used as a secondary reference in this study.

Ongur (1972) made a volcanologic investigation in the Dikili-Bergama region. After geophysical and geochemical investigations, he pointed out the high geothermal potential of the area. Gerhard (1972) discussed the geology of metasomatic iron deposits in Balikesir province. Krushensky (1976) , after studying volcanic and plutonic rocks in the study area, suggested their origin to be a subduction zone,

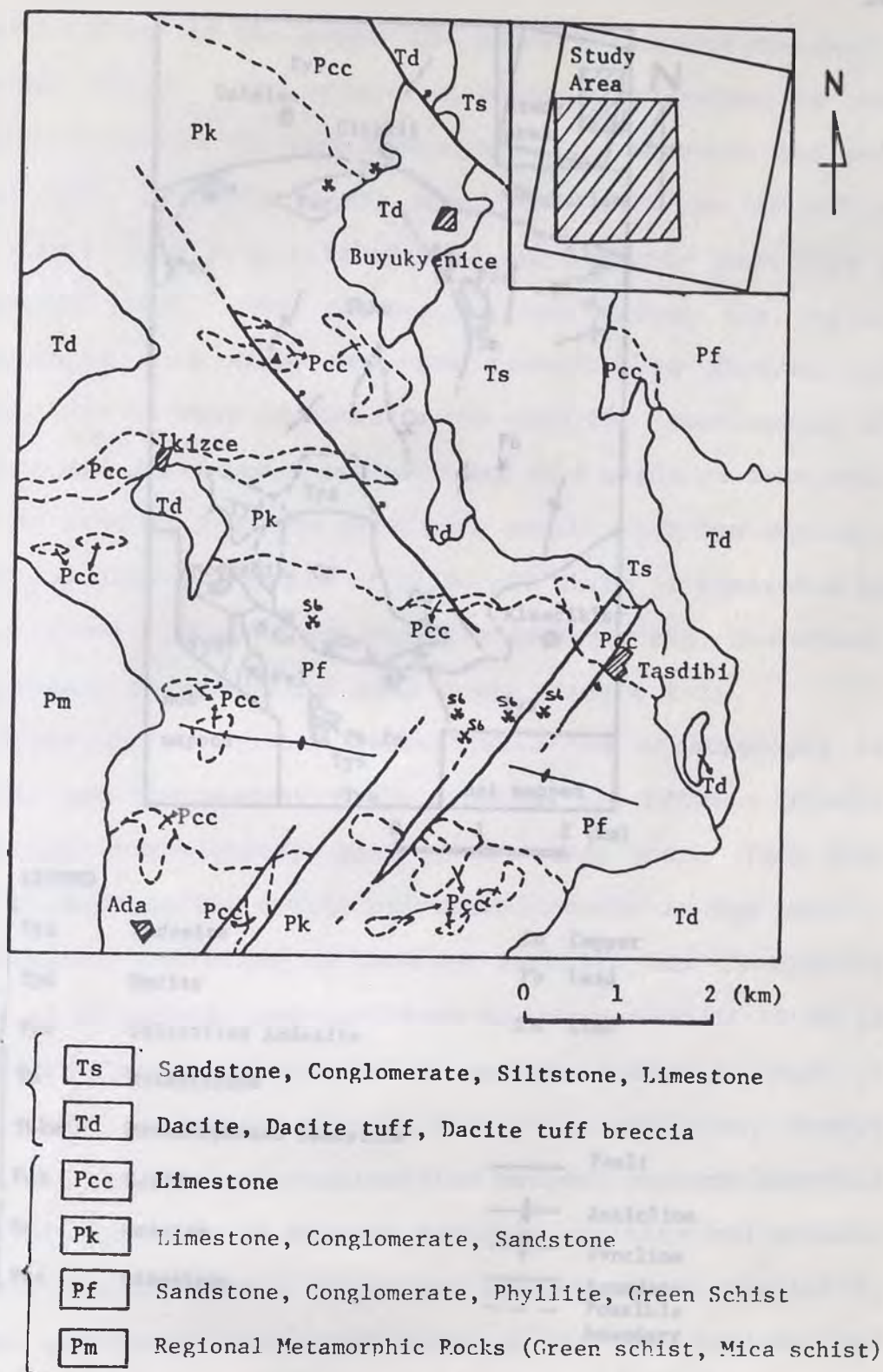
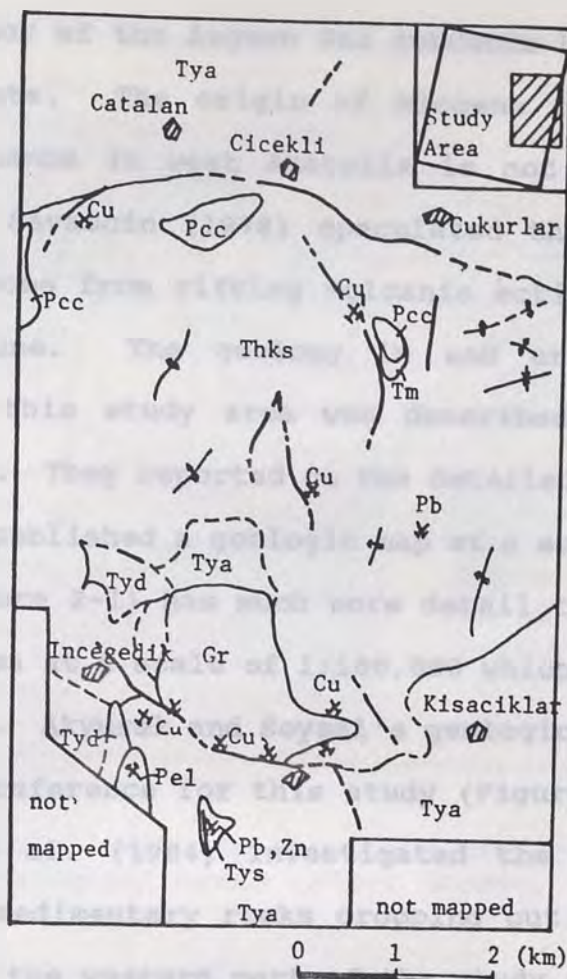


**Figure 2-3.** Geologic map of a part of the study area (modified from Mariko, 1970).



LEGEND

Tertiary	Tya	Andesite	Cu	Copper
	Tyd	Dacite	Pb	Lead
	Tys	Silicified Andesite	Zn	Zinc
	Tm	Metadiabase		
	Thks	Metamorphosed Sandstone		
Permian	Pel	Perlite	—	Fault
	Gr	Granite	↕	Anticline
	Pcc	Limestone	∩	Syncline
			—	Boundary
			- - -	Possible boundary

Figure 2-4. Geologic map of a part of the study area (modified from Ozcan, 1972).

where the floor of the Aegean Sea subducts beneath the West Anatolian Plate. The origin of Miocene calc-alkaline and alkaline volcanos in west Anatolia is not certain and not agreed upon. Savascin (1978) speculated that the volcanics more likely come from rifting volcanic activity than from a subduction zone. The geology in and around the region encompassing this study area was described by Akyurek and Soysal (1981). They reported on the detailed stratigraphy of the area and published a geologic map at a scale of 1:25,000. This map (Figure 2-1) has much more detail than the geologic map of the area at a scale of 1:100,000 which is published by M.T.A. (1989). Akyurek and Soysal's geologic map, therefore, is a primary reference for this study (Figure 2-2).

Ercan et al. (1984) investigated the stratigraphy of magmatic and sedimentary rocks cropping out between Edremit and Korucu in the western part of the study area. They also tried to explain the origin of volcanic rocks in the region. The tectonic evolution of western Anatolia was studied by Sengor et al. (1985) who explained the formation of 10 to 11 major host-graben structures in western Anatolia, most of which trend east-west (Figure 2-5). In addition, Sengor (1987) has pointed out similarities between western Anatolia and Nevada in terms of Neogene tectonic activity and graben-bounding faults. Larson (1989) has emphasized the similarity of the geothermal situation between the two regions and speculated on the gold potential of western Anatolia. These similarities suggest that gold mineralization in western

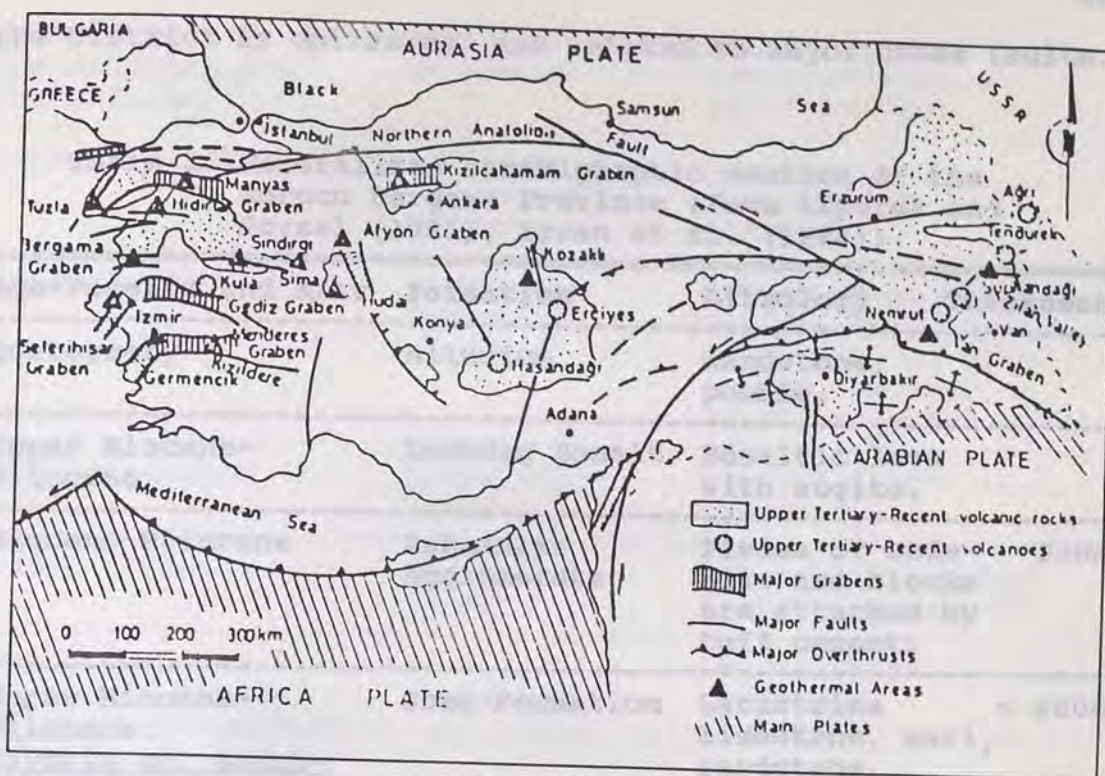


Figure 2-5. Recent tectonic structure of Turkey and geothermal areas (after Larson, 1989).

Anatolia is highly probable.

Recently, Erler and Larson (1990) provided a genetic classification of gold occurrences in the Aegean Region, Turkey. They pointed out that host rocks of gold mineralization include Tertiary volcanics, silicified limestones, ophiolite and melange-associated sequences, and the metamorphic rocks of the Menderes Massif. They studied the Ivrindi District, located slightly north of the study area, as a part of their paper. According to Erler and Larson (1990), mineralization occurs in dacitic to andesitic volcanics where they are generally silicified, pyritized and argillically altered. They concluded that metal deposition in

the District is epithermal and related to major cross faults.

**Table 1.** Generalized stratigraphic section of the Korucu Bergama Province (from Akyurek and Soysal (1981), Ercan et al. (1984)).

Age-Fossils and K/Ar	Formation	Lithology	Thickness
Quaternary	Alluvium	Sandstone, pebble.	
Upper Miocene- Pliocene	Dededag Basalt	Basaltic lava with augite.	
Miocene-Pliocene	Rahmanlar Agglomerate	Pieces of ande- site and blocks are attached by tuff cement.	200m
Upper Miocene- Pliocene: <u>Cypria cf. ophth-</u> <u>almica Jurine, Candona</u> <u>neglecta Sars, Cypri-</u> <u>notus cf. solinus</u> <u>Brady, Ilvocypris</u> <u>brady Sars.</u>	Soma Formation	Lacustrine limestone, marl, sandstone, tuffite.	< 400m
Upper Miocene	Ballica Formation	Conglomerate, sandstone	50-60m
Miocene-Pliocene	Yunutdag Volcanics	Andesite, tuff, silicified tuff, lahar, basalt.	
Lower Miocene: K/Ar	Yurekli Dacite	Dacite, rhyodacite, rhyolite.	500m
Middle Triassic (Anisian): <u>Endothyranella wirzi</u> <u>Kohen-Zaninetli.</u> <u>Trochammina cf almta-</u> <u>lensis Koehn-Zanin-</u> <u>etti, Aqathammina sp.</u>	Kapikaya Formation	Conglomerate, limestone, sandy- limestone, sandstone.	
Eocene-Oligocene: K/Ar	Kozak Granodiorite	Granodiorite, monzogranite, porphyricgranodiorite.	

Lower Triassic: <u>Meandrospira cf.</u> <u>Pusilla (Ho)</u>	Kinik Formation	Metasandstone, metamudstone, metavolcanics.
Lower Triassic	Bakirtepe Volcanics Member	Metesplite, metadiabase, metatuff.
Lower Triassic	Cavdarstepe Formation	muscovite-quartz schist, sericite- chlorite schist, quartz- actonite schist.
Lower Triassic	Ayclitepe Member	Crystallized limestone.
Lower Triassic	Kocacukur Member	Metaspilite, meta- diabase, metatuff.
Upper Permian: <u>Dunbarula tumida</u> <u>Skinner, Verbeekina</u> <u>verbeeki Geintz.</u> <u>Chusenella sp.</u>	Caldag Limestone	Grey colored limestone.

KINIK FORMATION (TKK) - This formation is exposed along the east side of the study area, almost from its north to south limits. Another part of the formation (the Tuzkall Mountains) trends from east to west in the middle of the study area. The formation consists of metabasites and metasediments that

## GEOLOGIC FORMATIONS

The following geologic information about the study area is summarized from Akyurek and Soysal's work (1981).

## PERMIAN ROCKS

**CALDAG LIMESTONE (Pcc)** - This allochthonous unit is distributed as blocks on the Kinik Formation. It is a grey, unmetamorphosed, crystalline limestone. It has a rich variety of fossils. Fossils define this unit's age as Upper Permian.

## TRIASSIC ROCKS

**CAVDARTEPE FORMATION (Thc)** - This unit is in the southwest section of the study area. Regional metamorphism of pelitic and psammitic rocks to the greenschist facies resulted in muscovite-quartz schist, sericite-chlorite-quartz schist, sericite-chlorite schist, biotite quartzite, quartz-albite-biotite schist, quartz-epidotite-chlorite schist. It is conformably overlain by the Kinik Formation. The unit is non-fossiliferous. The age of the Kinik Formation, based on fossils (Table 1), is Lower Triassic, so the Cavdartepe Formation's age is Lower Triassic.

**KINIK FORMATION (Thk)** - This Formation is exposed along the west side of the study area almost from its north to south limits. Another part of the Formation (the Turkali Mountains) trends from east to west in the middle of the study area. The Formation consists of metasandstones and metamudstones that



are slightly metamorphosed to the greenschist phase.

The Kinik Formation conformably overlies the Cavdartepe Formation. The Kinik Formation is very poor in terms of fossils. Only Menadrosina cf. and pusilla (Ho) indicative of Lower Triassic were found in the sandy limestone bands in the unit.

BAKIRTEPE VOLCANIC MEMBER of HALILAGA GROUP (Thkb) - This member is composed of spilite, diabase and tuff which were metamorphosed to the greenschist facies. Spilites have gas holes filled by calcite. This member is nonfossiliferous. Permian Limestone allochthonous blocks overlie this unit.

TERTIARY ROCKS  
YUNUTDAG VOLCANICS (Tyu) - The volcanics cover the southeast section of the range, and consist of andesite, andesitic tuff, tuff, silicified tuff, lahar, and basalt.

The andesite appears in grey and yellow, and locally shows different mineralogic composition ranging from trachyandesite to trachyte. It generally includes large glassy plagioclase phenocrysts, and primary flowing bands are present. It has porphyritic texture and has been chloritized, argillized, and carbonated. It contains andesine, biotite, and opaque minerals. Tuffs are sometimes completely kaolinised.

Silicified tuffs, sometimes perlitic, appear in different colors (Figure 2-4).

The lahar lithology is composed of middle to large pebbles and blocks of andesite which are cemented by tuff.

The Yunutdag volcanics can be seen under, and over, and sometimes merge with the Soma Formation. These volcanics were started before sedimentation of the Soma Formation and were continued during the sedimentation.

These volcanics are a result of the second period of volcanic activity which started before Miocene and ended during the Upper Miocene-Pliocene (Ercan et al., 1984).

**SOMA FORMATION (Ts)** - This Upper Miocene-Pliocene unit is the second most widespread formation in the study area, it occurs in the middle of the area almost from its north edge to its south boundary. The Formation consists of alternating fossiliferous lacustrine limestone, clay, marl, sandstone and tuffite. It is generally yellow, grey or white, and exhibits thin to thick layering. The Formation is generally horizontal or almost horizontal, but it is tilted and sometimes folded. Tuffs are generally altered to kaolinite. Locally some coal and bituminous shale are founded in the Formation. Beyond the boundaries of the study area its thickness reaches 400 m (Ercan et al., 1984).

It directly covers the Kinik Formation and the Yunutdag Volcanics. The Soma Formation mixes with the Rahmanlar Agglomerate, and is covered by the Dededag Basalt out of the study area.

RAHMANLAR AGGLOMERATE (Tr) - This rock type, formed after the Yurekli Dacite is exposed in the southern part of the study area. It consists of tuff cemented andesite-dacite-rhyodacite pebbles. Tuff and siltstone layers are generally located between agglomerate blocks. Its thickness is approximately 200 m (Ercan et al., 1984). The unit overlies the Yunutdag Volcanics and locally overlies the Soma Formation. It unconformably overlies the Kinik Formation. Its age is probably Upper Miocene-Lower Pliocene.

## CHAPTER III

## METHODOLOGY

## TM MISSION AND RATIONALE FOR TM DATA

The availability of Landsat TM data since 1982 has improved the efficiency of satellite remote sensing in geological applications. There have been a total of five Landsat vehicles launched by NASA since 1972. Landsat 1, 2, and 3 circled the earth at 918 km recording reflected radiation from a multispectral scanner (MSS) in two visible and two near infrared reflected radiation bands. Recognizing the popularity and potential of sensors like Landsat MSS (1, 2, and 3), NASA also launched (1982 and 1985) Landsat 4 and 5, which differ from previous missions in orbit, design, and sensor capabilities. These advanced satellites carry a payload that includes a higher resolution sensor called the Thematic Mapper (TM). Major improvements of TM over conventional MSS data are:

1. Increased spatial resolution (30 m).
2. Improved spectral separation.
3. Expanded spectral range (7 bands).
4. Improved radiometric resolution.
5. Collection of both reflected and thermal data.

Sensor details are given in the Appendix. TM, as noted, provides image data at a better ground resolution than is possible with MSS sensors. Data is collected for seven different bands which were chosen to improve identification of

surface cover. To create an image with ground resolution of 30 m (98 ft), a 16-element detector is used. Especially noteworthy is TM's abilities to record thermal radiation at the 10.4-12.5 micron wavelengths. However, data recorded in this part of the spectrum yield a poorer ground resolution of 120 m (390 ft). Because TM collects information in seven different bands, one has the opportunity to select a variety of band combinations.

#### ATMOSPHERIC CORRECTION

Atmospheric scattering results from multiple interactions between light rays and the gases and particles of the atmosphere (Sabin, 1987). This scattering can be divided in two sections; selective scattering and nonselective scattering. Selective scattering predominates in the blue wavelength portion of the spectrum and is caused by smoke, fumes and gases. In the case of nonselective scattering all wavelengths in the visible section of light are equally scattered and cause an effect on the image that is called "haze". This haze effect results in some extra illumination that reduces the contrast difference among substances in an image, thereby reducing the spatial resolution and detectibility of the image. This scattering is caused by dust and water droplets.

The total scattering affects blue wavelengths at least twice as strong as it does red light (Sabin, 1987). Therefore, TM band 1 (0.45-0.52  $\mu\text{m}$ ) is affected the most by

scattering. To correct this unwanted atmospheric effect some techniques have been developed. One of these techniques is based on the fact that TM band 7 is essentially free of atmospheric effect (Sabins, 1987). This can be verified by examining the digital numbers (DNs) corresponding to bodies of clear water and shadows. Both water and deep shadows have values of either 0 or 1 on TM band 7. This technique employs an area within the image that has shadows caused by irregular topography or deep water. For each pixel the DN in band 7 is plotted against the DN in band 1, and a straight line is fitted through the plot, using a least-squares technique. If there were no haze in band 1, the line would pass through the origin; but the haze causes an intercept offset along band 1 axis. To correct the haze effect on band 1, the value of the intercept offset is subtracted from the DN of each band 1 pixel for the entire image.

Another atmospheric correction method was developed by Crippen (1987), and is referred to as the "regression intersection method". I used this technique which is simple and straightforward. It is also based on the idea that TM band 7 is free of haze and atmospheric influence. To determine the correction amount (DN values) for any TM band, say TM band 1, make a ratio image  $TM1/TM7$ . If there were no haze in TM 1, the topography in the ratio image would be suppressed. If there were some haze in band 1, shadows in TM 1 or TM 7 would be shown reversed in the ratio image. Employing trial-errors technique, first a correction DN value

for band 1 was predicted and subtracted from each pixel in the TM band 1, then again a TM1/TM7 ratio image was prepared by using the new band 1. The process was repeated until all topographic effects suppressed in the ratio image. TM bands 1, 2, 3, 4, and 5 were corrected by employing this technique.

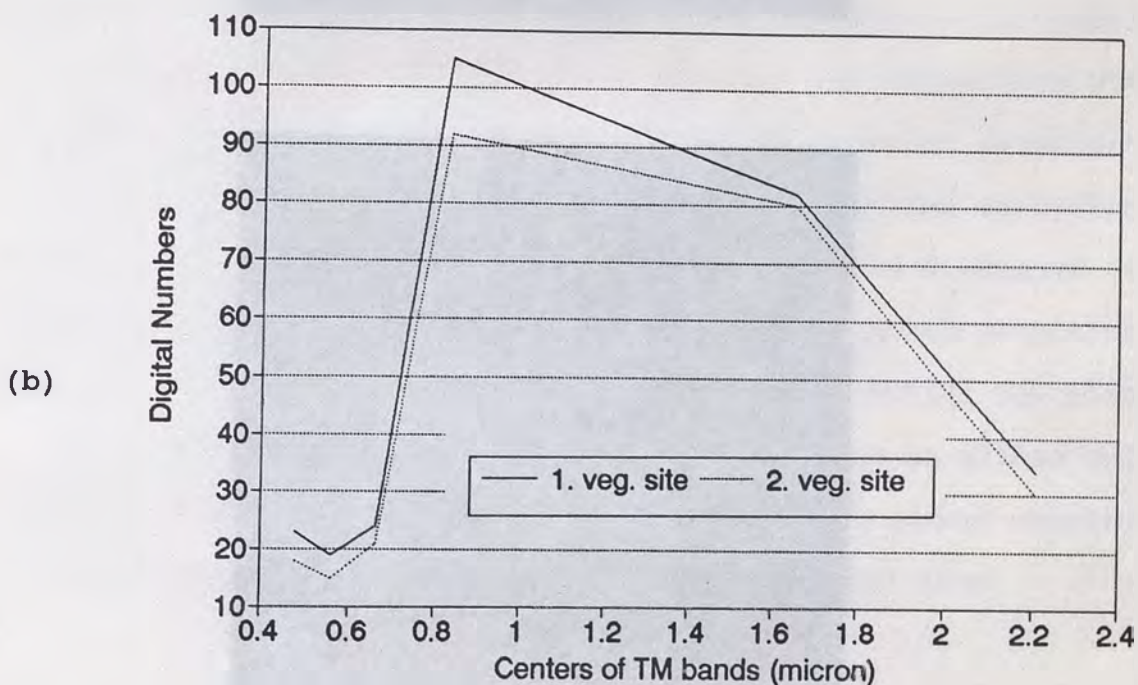
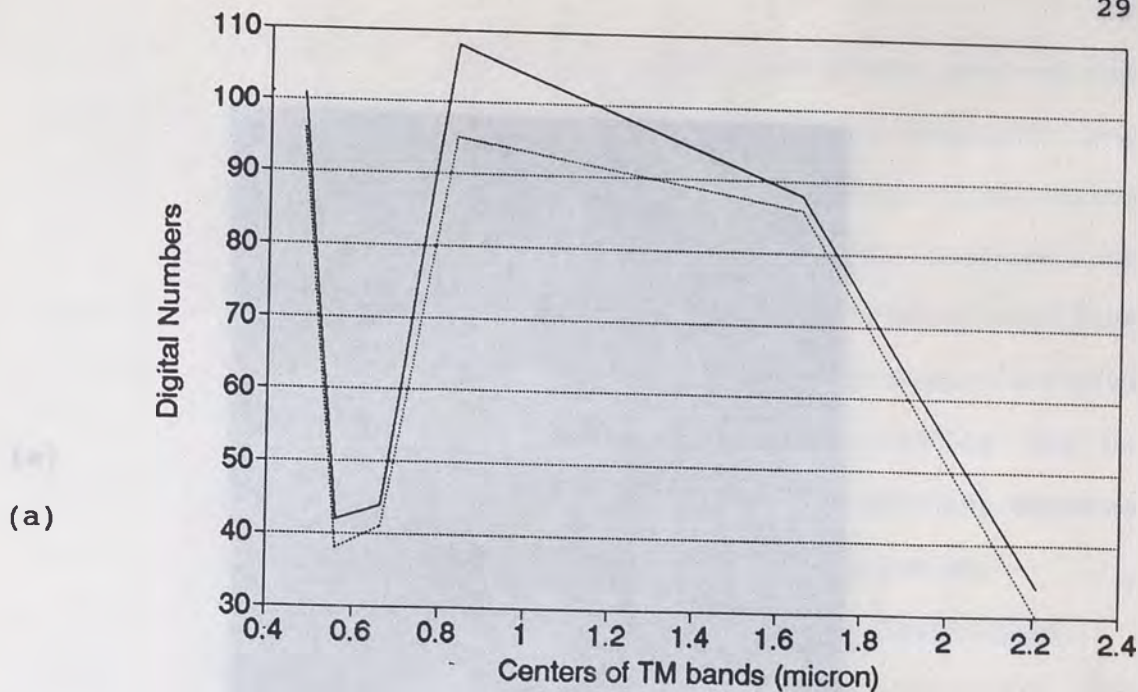
Crippen (1988) discussed the danger of over looking this correction on ratio images, and he showed how it could lead one to misinterpretation of a ratio image.

Figure 3-1 shows DNS of TM bands for two agricultural areas in the study area before and after atmospheric correction. Figure 3-2 shows a color composite of TM bands 3, 2 and 1 in red, green and blue (RGB) before and after atmospheric correction. Note the bluish haze which dominates the image before atmospheric correction.

#### IMAGERY ANALYSIS

Imagery analysis was conducted on the Mackay School of Mines' VAX 11/780 based Electromagnetic Systems Laboratories Interactive Digital Image Manipulation System (IDIMS). The IDIMS software package contains over 250 application functions.

The Landsat TM image of western Turkey (21 August 1986, Path 180, Row 33) was obtained with a sun elevation angle of  $51^\circ$  and a sun azimuth angle of  $125^\circ$ . Image analysis was made on a 512 x 512 subscene. Although individual minerals can not be distinguished by TM sensors due to poor spectral and spatial resolutions, altered and unaltered rocks are distin-



**Figure 3-1.** a) Uncorrected Landsat TM digital numbers (DNs) for bands 1, 2, 3, 4, 5, and 7 plotted at band center wavelengths for two agricultural areas ("veg. sites"). b) corrected DN's for the same sites. Note especially, the removal of haze in the shorter wavelength region.



(a)



(b)



**Figure 3-2.** Images of study area, a) Color composite of TM bands 3, 2 and 1 (in RGB) before atmospheric correction, b) after atmospheric correction. Note bluish haze in (a).

guishable (Chapter V). After analyzing the chosen area on the image manipulation system, subsequent field sampling was designed. Sample sites were selected to include distinctive remote sensing units in terms of color, tone, texture, or pattern characteristics. Further image processing was then applied in the Fall of 1991, after the previous summer's field work. The aim of subsequent imagery manipulation was to refine enhancement techniques and to maximize contrast between rock units with the help of direct field experience.

For the study area, the image processing techniques listed in Table 2 were produced and photographed with the system's Dunn camera on 35 mm film. Image composites other than those listed in Table 2 were reviewed, but those from the table were determined to represent the best contrast relationships between lithologies. The rationale behind the selection of these bands and enhancement techniques will be discussed in subsequent chapters. Each individual band image and composite image was contrast stretched, using the IDIMS REDIST function usually at a 0.2 truncation of brightness values at either end of the brightness range. All composites were color encoded using the three primary colors, red, green, and blue.

## FIELD INVESTIGATION

Figure 2 shows the data during the summer of 1981. Approximately 20 samples were collected from 20 sites (Figure 3-3).

**Table 2.** Landsat 5 Thematic Mapper images and image composites analyzed at the study area. All composite images are color encoded in red, green, and blue (RGB).

INDIVIDUAL BANDS: 1,2,3,4,5,7

SINGLE BAND COMPOSITES: 5,4,1; 3,2,1; 4,3,2; 2,4,7

RATIO COMPOSITE: 3/1,4/3,5/7

ISH: TM band composite of 3,5,7 and 1,3,5

PRINCIPAL COMPONENTS: Individual PCs 1,2,3,4,5,& 6

PRINCIPAL COMPONENTS COMPOSITES: 1,2,3; 2,3,4; 2,4,5

SELECTED PRINCIPAL COMPONENTS: The fourth components of PC transformation of TM 1,3,4,5 and TM 1,3,5,7

DECORRELATION STRETCH: Individual DSs 1,2,3,4,5,& 6

DECORRELATION STRETCH COMPOSITE: 4,5,6

COMPLEX COMPOSITES: SPC4 (bands 1,3,4,5) SPC4 (bands 1,3,5,7)-PC4

### FIELD INVESTIGATION

Field work was done during the summer of 1991. Approximately 55 samples were collected from 20 sites (Figure 3-3). Most sites were photographed. An attempt was made to acquire reasonably complete sample coverage from both an imagery and a lithologic perspective. Ground based 35 mm photographs were taken to encompass representative scenes including outcrop, soil and vegetation.

### LABORATORY SPECTROMETER MEASUREMENTS

Laboratory spectral measurements were made over visible and infrared wavelength regions to cover the same spectral region as the TM. These spectra were used to identify the lithologic unit and alteration types of the samples. Over 20 samples, which represent some formation units, and alteration, were measured using a Beckman 5240 spectrometer at the Desert Research Institute (DRI), Reno. The Beckman spectrometer measures bidirectional reflectance in visible and near- and mid-infrared wavelengths (400 nm to 2500 nm), with a spectral resolution of 1 % of the wavelength.

The positions of spectral absorption features measured in the laboratory were compared to published laboratory and field spectra (Hunt and Ashley, 1979; Hunt, 1979; Hunt and Salisbury, 1974; Hunt et al., 1973; Hunt and Salisbury, 1970; Salisbury et al., 1987; and Collins, 1988).

CHAPTER 3

MINERAL CHARACTERIZATION

Although there is not a direct relationship between laboratory spectra of rocks and the in the sample data, some useful information can be extracted from laboratory spectra to improve our understanding of the characteristics of formations in an area. Therefore, the characteristic laboratory spectra of rocks which are related to the formation of the study area are presented in this chapter.



Figure 3-3. Location of sample sites in the study area.

## CHAPTER IV

## SPECTRAL CHARACTERISTICS

Although there is not a direct relationship between laboratory spectra of rocks and DN's in TM image data, some useful information can be extracted from laboratory spectra to improve our understanding about characteristics of formations in an image. Therefore, this chapter reviews basic laboratory spectral characteristics of rocks and minerals which are related to the study area and attempts to make a connection between laboratory spectra of the rocks and DN's of TM bands. This approach can help to explain color hues in color composite images in the next chapter.

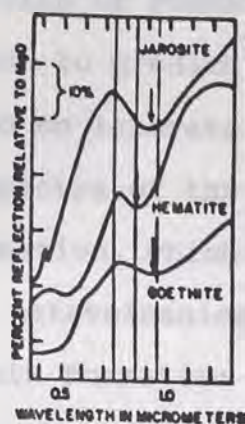
## BASIC SPECTRAL CHARACTERISTICS OF ROCKS

Various characteristics of ions and molecules may cause characteristic spectral features of rocks. In the visible spectrum, some mineral species can be any of several colors depending on trace element content or isomorphous element ratios (Spatz, 1988). There are two fundamental interatomic and intermolecular processes that control mineral and rock spectra: electronic and vibrational (Hunt, 1980).

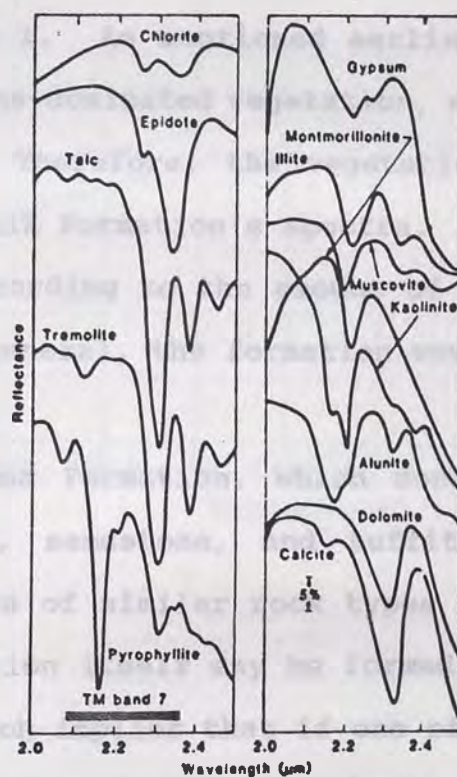
Excitation of electrons in the atomic structure causes transitions in energy levels, which is called the electronic process (Hunt, 1980). Absorption features at wavelengths shorter than  $1.2 \mu\text{m}$  (1200 nm) include electronic transitions involving iron (Hunt and Ashley, 1979). Iron-oxide spectra

exhibit a rapid falloff toward the near-ultraviolet because of intense absorption due to electron transfer between two ions. Overprinted on the intense absorption feature are features due to ferric ion crystal field transitions (Hunt and Ashley, 1979). In hematite, the predominant transition is centered near  $0.85 \mu\text{m}$ , while in goethite it is centered near  $0.94 \mu\text{m}$ . The shoulder near  $0.65 \mu\text{m}$  is most apparent in goethite. In jarosite, a transition feature near  $0.43 \mu\text{m}$  is unusually sharp (Figure 4.1).

Many absorption features at wavelengths of  $1.2$  to  $2.5 \mu\text{m}$  are due to vibrational transitions of the hydroxyl ( $\text{OH}^-$ ) groups (Hunt and Ashley, 1979). Vibrational behavior is caused by electronic instability between the molecule and the surrounding electronic field. The most useful wavelength region for identifying alteration minerals is the  $2.0$  to  $2.5 \mu\text{m}$  region. Between  $2.16$  and  $2.23 \mu\text{m}$ , absorption minima are caused by combinations of the OH-band fundamental stretch with the Al-O-H fundamental bending mode (Figure 4-2) (Hunt and Ashley, 1979). These minima are diagnostic of aluminum-bearing clays which commonly occur in **hydrothermally altered rocks**. The absorption feature may appear as a sharp, broad, or multiple minimum, depending on the structure of the mineral. Montmorillonite has a broad minimum at  $2.21 \mu\text{m}$ . kaolinite and alunite have doubled features centered at  $2.21 \mu\text{m}$  (Figure 4.2). Carbonate minerals show strong absorption features near  $2.35 \mu\text{m}$  caused by vibrations of the carbonate group (Hunt and Ashley, 1979) (Figure 4-2).



**Figure 4-1.** Features due to electronic transitions in the spectra of iron-bearing minerals. Spectra are displaced vertically, and characteristic features are indicated by arrows (after Hunt and Ashley, 1979).



**Figure 4-2.** Selected laboratory spectra of minerals containing overtone vibrational absorption features for Al-OH (2.16 to 2.22  $\mu\text{m}$ ), Mg-OH (2.3 to 2.35  $\mu\text{m}$ ), and CO (2.3 to 2.35  $\mu\text{m}$ ). TM band 7 is indicated (after Goetz, Vane, Solomon and Rock, 1985).



## SPECTRAL CHARACTERISTICS OF FORMATIONS IN THE STUDY AREA

An attempt was made to predict characteristics of rocks in the study area based on laboratory spectra of samples and previously published spectra of the same kind of rocks.

For the Kinik Formation, which is composed of metasandstones, metamudstones, metavolcanics, spectra of sample sites 20 and 21 from the Kinik Formation are shown in Figure 4.3. Metamorphic rocks have a diagnostic reflectance minimum around  $2.35 \mu\text{m}$  in general due to opaque and carbonate minerals (Hunt and Ashley, 1976). According to these spectral characteristics, the Kinik Formation would have high values in TM band 5 and low in band 1. As mentioned earlier, the formation is overlain by a pine-dominated vegetation, ranging in cover from 40 % to 70 %. Therefore, the vegetation spectra would be added to the Kinik Formation's spectra. These mixed spectra would change according to the amount of vegetation over the formation. In general, the formation would show up brighter in TM 3/1 image.

For the Soma Formation, which consists of lacustrine limestone, marl, sandstone, and tuffite, some previously published spectra of similar rock types are shown in Figure 4-4. The formation itself may be formed by one or a few of these units, which implies that if one of these subunits has a large enough exposure and concomitant diagnostic spectral characteristics, it would be distinguishable in the color composite images. A chosen spectra from sample site 15 is shown in Figure 4-5. In general the formation would have high

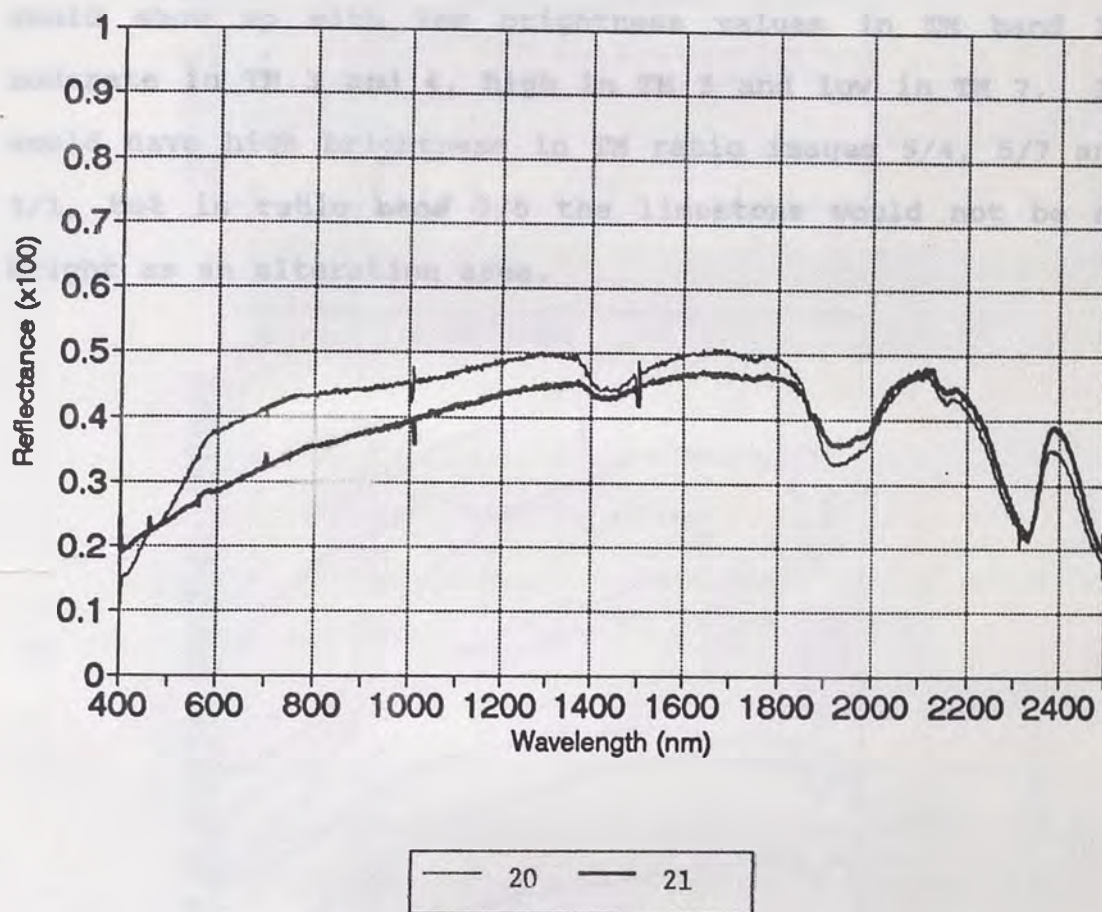


**Figure 4-3.** Beckman laboratory spectra of samples from sample sites 20 and 21 from the Kinik Formation. Note the carbonate absorption near 2.35  $\mu\text{m}$ .

brightness values in TM bands 5 and 7, moderate in 4 and 3.

For the Caldag Limestone Member, published laboratory spectra of limestones are shown in Figure 4-4b, and a laboratory spectrum of a sample from sample site 14, which was mapped as Caldag limestone, is shown in Figure 4-6. Both laboratory spectra have "classic" limestone signatures around  $2.35 \mu\text{m}$  wavelength due to carbonate minerals. The lithology would show up with low brightness values in TM band 1, moderate in TM 3 and 4, high in TM 5 and low in TM 7. It would have high brightness in TM ratio images 5/4, 5/7 and 3/1, but in ratio band 7/5 the limestone would not be as bright as an alteration area.

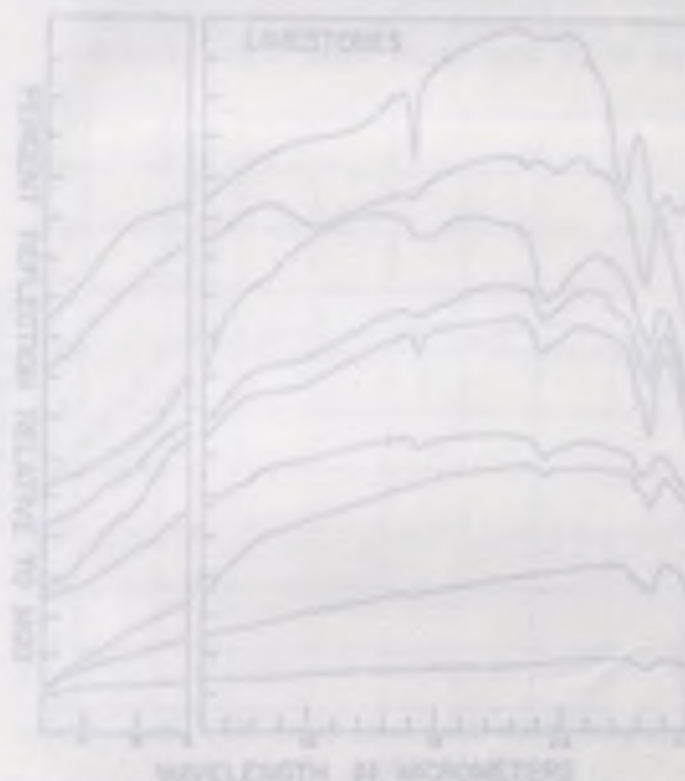


Figure 4-4. Published laboratory spectra of a variety of sandstones (a), and limestones (b). The spectra are displaced vertically, and percent reflectance markers are separated by  $10\%$  (from Hunt and Salisbury, 1976).

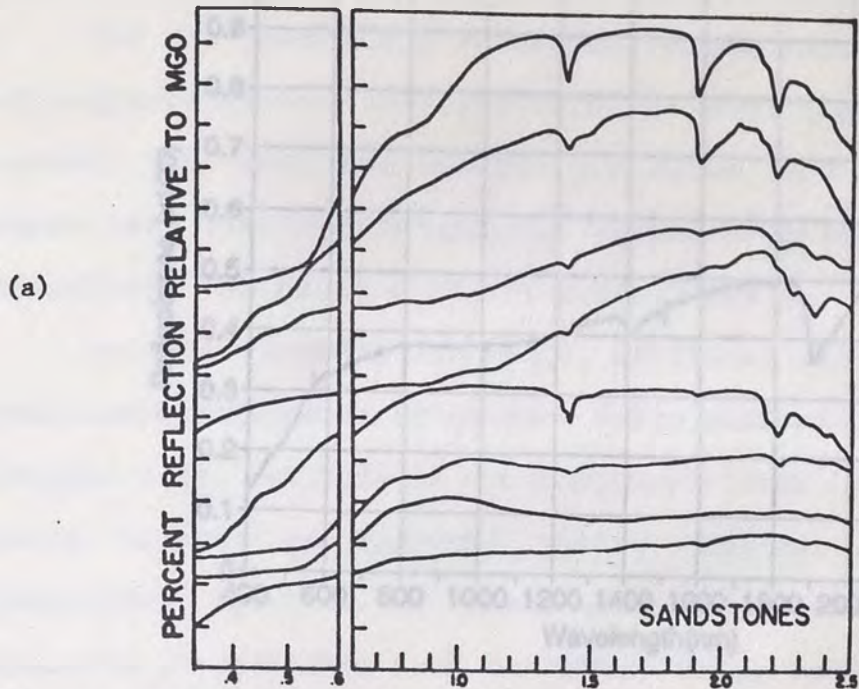


Figure 4-3. A chosen laboratory spectrum of a sample (a clay-carbonate rich sediment) from sample site 18, from carbonate rich sediment and 200 respectively.

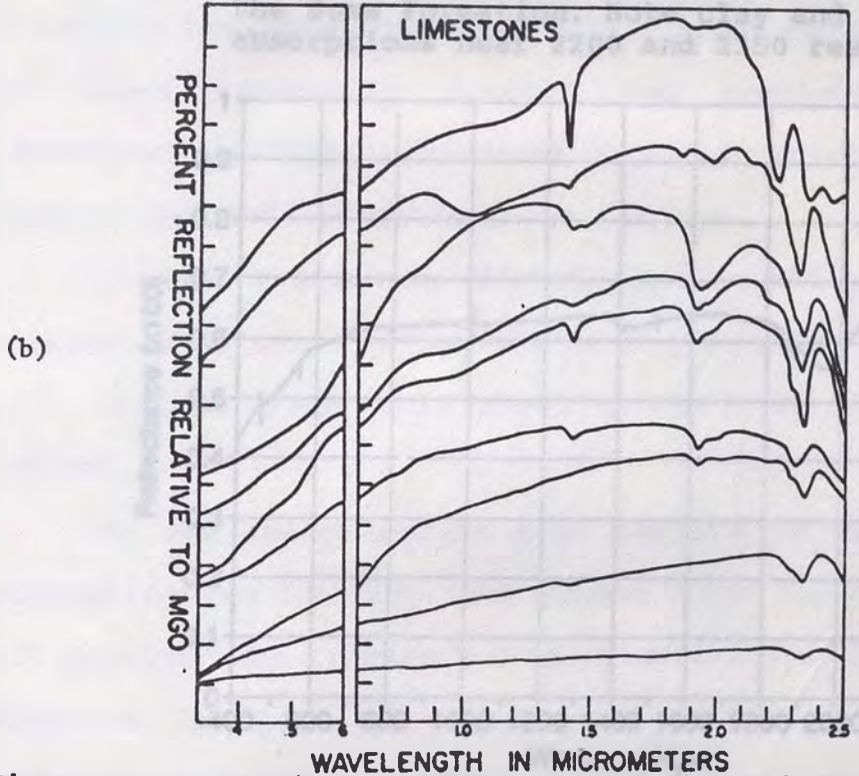
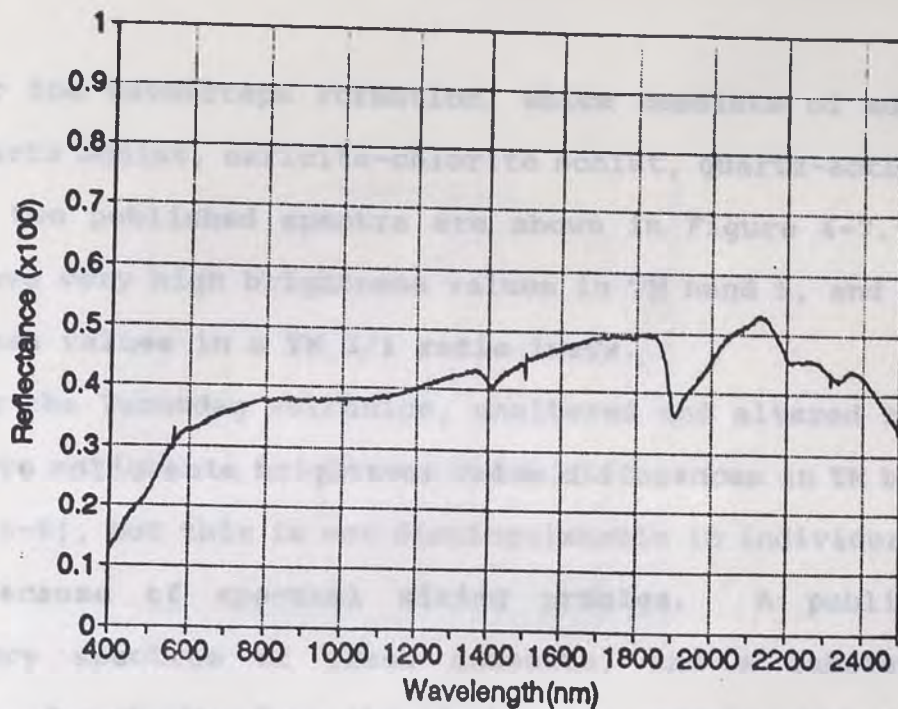
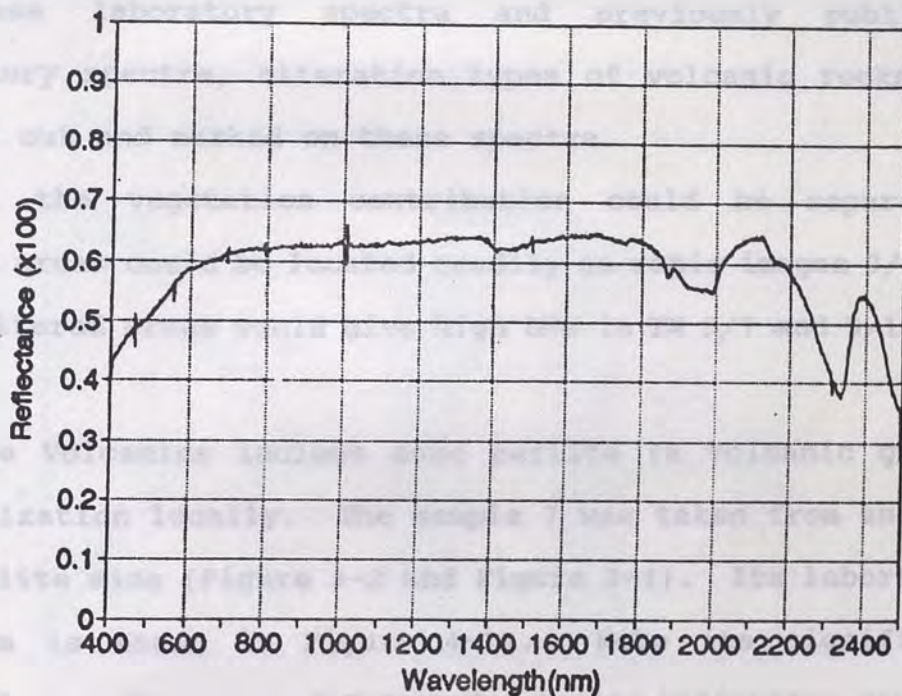


Figure 4-4. Published laboratory spectra of a variety of sandstones (a), and limestones (b). The spectra are displaced vertically, and percent reflectance markers are separated by 10 % (from Hunt and Salisbury, 1976).



**Figure 4-5.** A chosen laboratory spectrum of a sample (a clay-carbonate rich sediment) from sample site 15, from the Soma Formation. Note clay and carbonate absorptions near 2200 and 2350 respectively.



**Figure 4-6.** Laboratory spectrum (Beckman) of the Caldag Limestone Member. Note similar spectral characteristics with Figure 4-4b.

For the Cavdartepe Formation, which consists of muscovite-quartz schist, sericite-chlorite schist, quartz-actonite schist, two published spectra are shown in Figure 4-7. It would have very high brightness values in TM band 5, and high brightness values in a TM 3/1 ratio image.

For the Yunutdag volcanics, unaltered and altered rocks would have noticeable brightness value differences in TM bands (Figure 4-8), but this is not distinguishable in individual TM bands because of spectral mixing problem. A published laboratory spectrum of fresh andesite, and a laboratory spectrum of andesite from the study area, sample site 2 are shown in Figure 4-9. Spectra of sample sites from Yunutdag volcanics are shown in Figure 4-10. After careful comparison of these laboratory spectra and previously published laboratory spectra, alteration types of volcanic rocks are figured out and marked on these spectra.

If the vegetation contribution could be separated, altered areas could be located readily on ratio images 3/1 and 5/7. Altered areas would give high DNs in TM 5/7 and 3/1 band ratios.

The Volcanics include some perlite (a volcanic glass) mineralization locally. The sample 7 was taken from an open pit perlite mine (Figure 3-2 and Figure 2-4). Its laboratory spectrum is shown in Figure 4-11. Note its significant hydroxyl signature around  $2.2 \mu\text{m}$  due to its high water content (it has generally higher water content than obsidian; Dictionary of Geological Terms, Anchor Press, 1984).

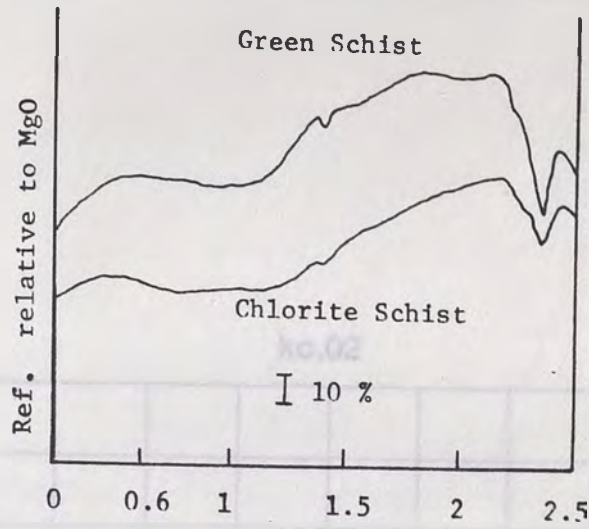


Figure 4-7. Published laboratory spectra of green schist and chlorite schist (modified from Hunt and Salisbury, 1976).

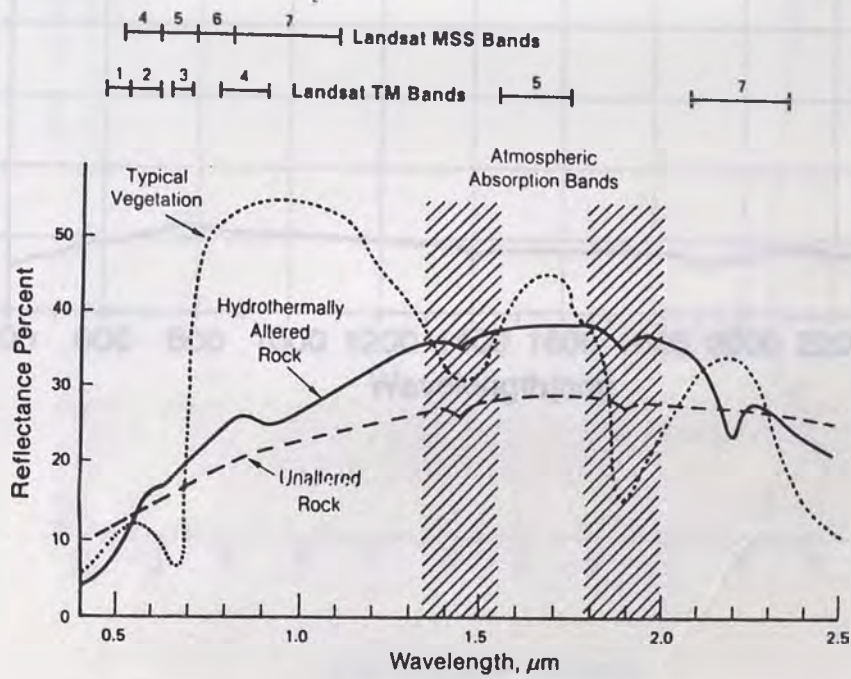
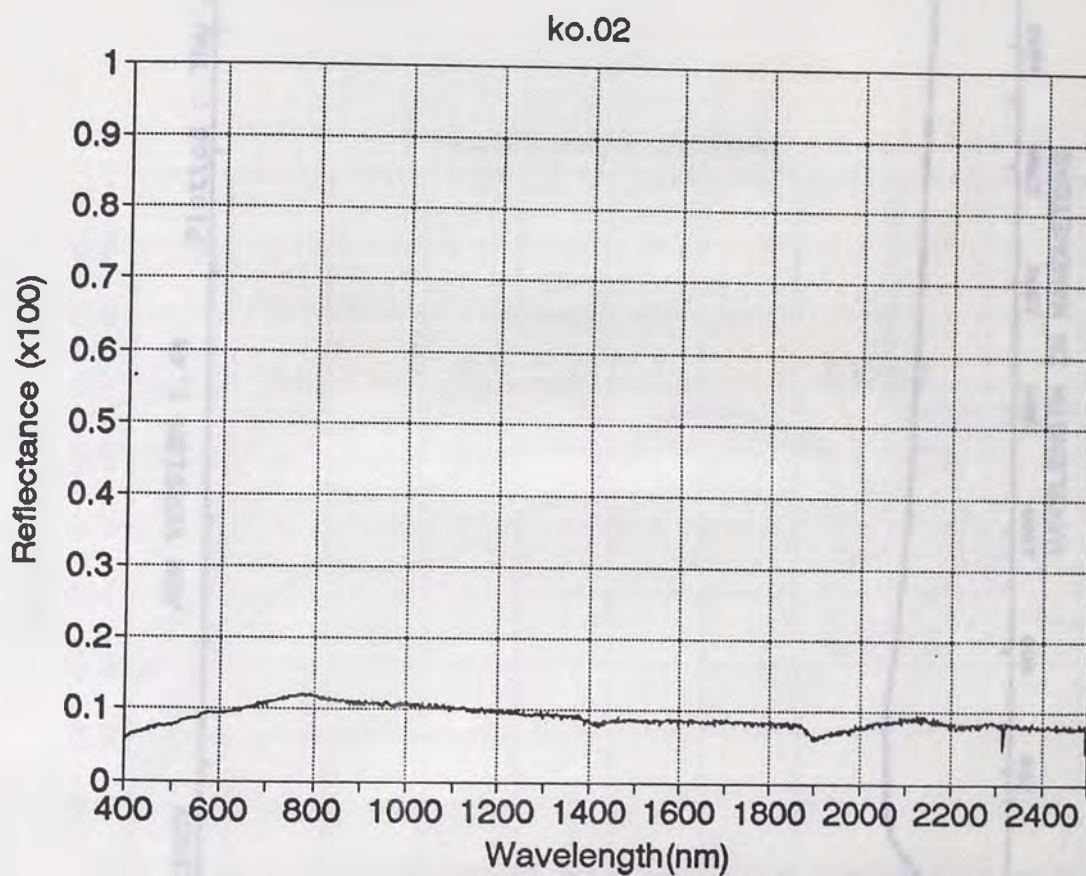
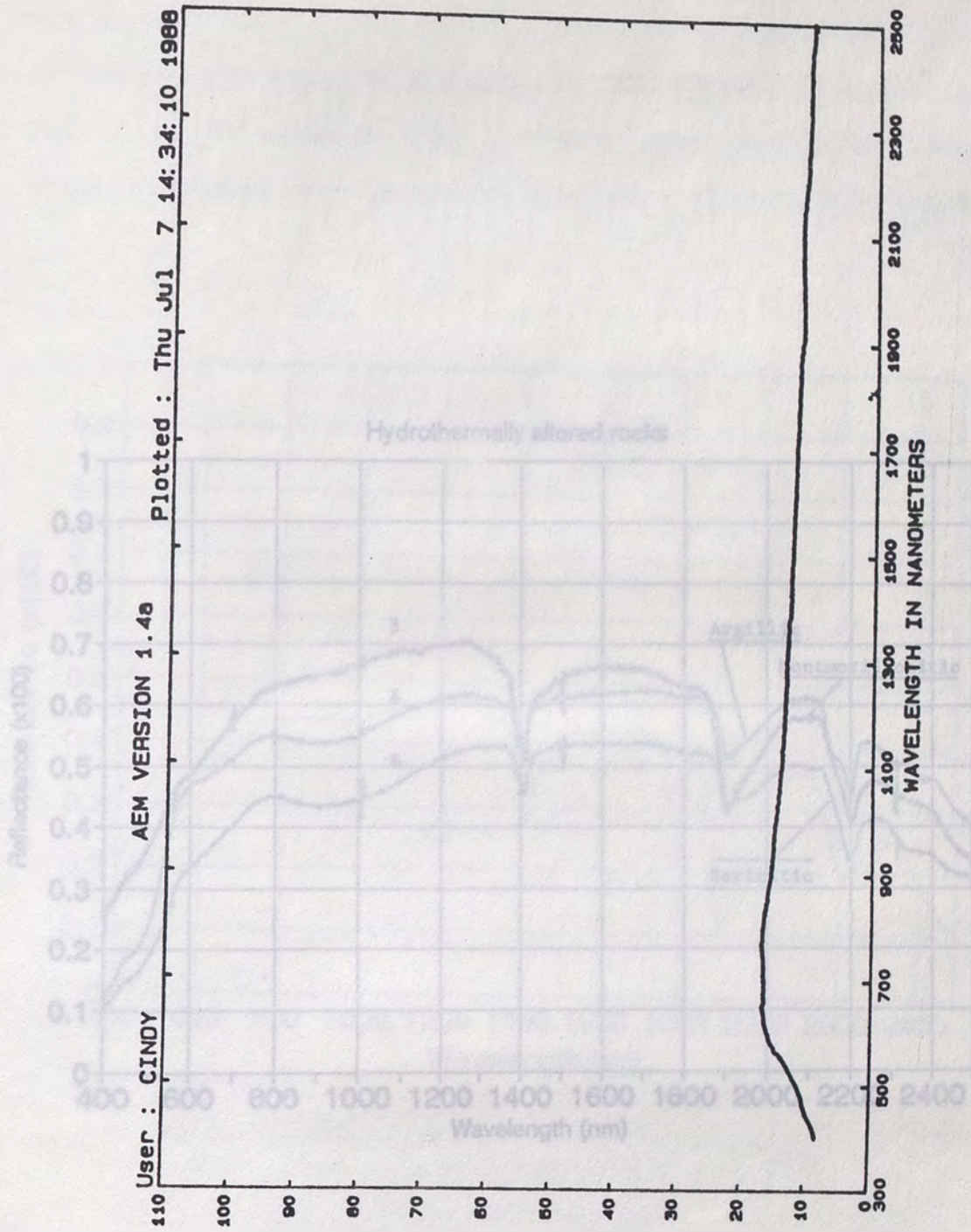


Figure 4-8. Reflectance curves for vegetation, unaltered rocks, and hydrothermally altered rocks (from Sabins, 1987).



**Figure 4-9a.** Laboratory spectrum of unaltered andesite from sample site 2 from the Yunutdag Volcanics. Compare with fresh andesite spectrum (4-9b).





PERCENT REFLECTANCE

Figure 4-9b. Published Beckman laboratory spectrum of fresh andesite (from Collins, 1988).

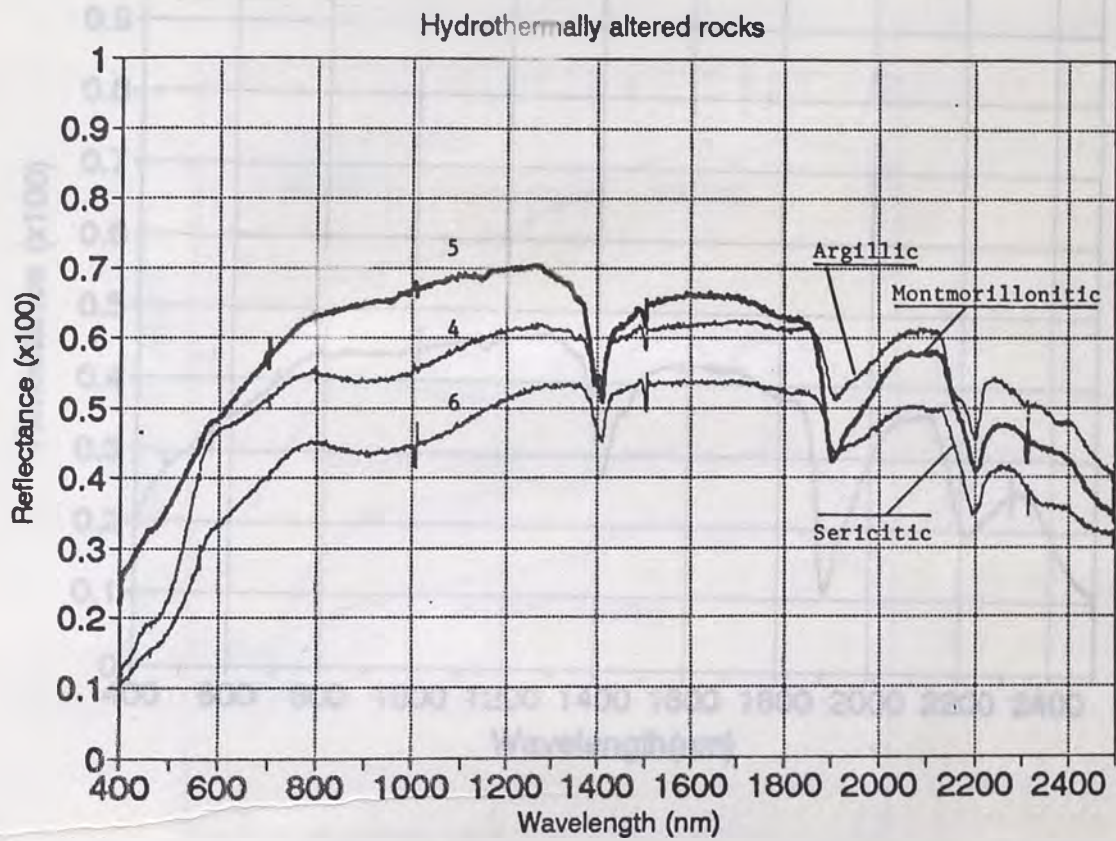


**Figure 4-10.** Laboratory spectra of samples from sample sites 4, 5, and 6 in the Yunutdag Volcanics. Alteration types indicated on spectra.

Oxton (1972) mapped a granite mass at the northwest of the town Turhall (Figure 2-4). Previously published spectra of granite are shown in Figure 4-12, and exhibit high spectral values in TW bands 5 and 7. These would appear as bright areas in single band images of TW 5 and 7 (Figure 5-1a and 5).

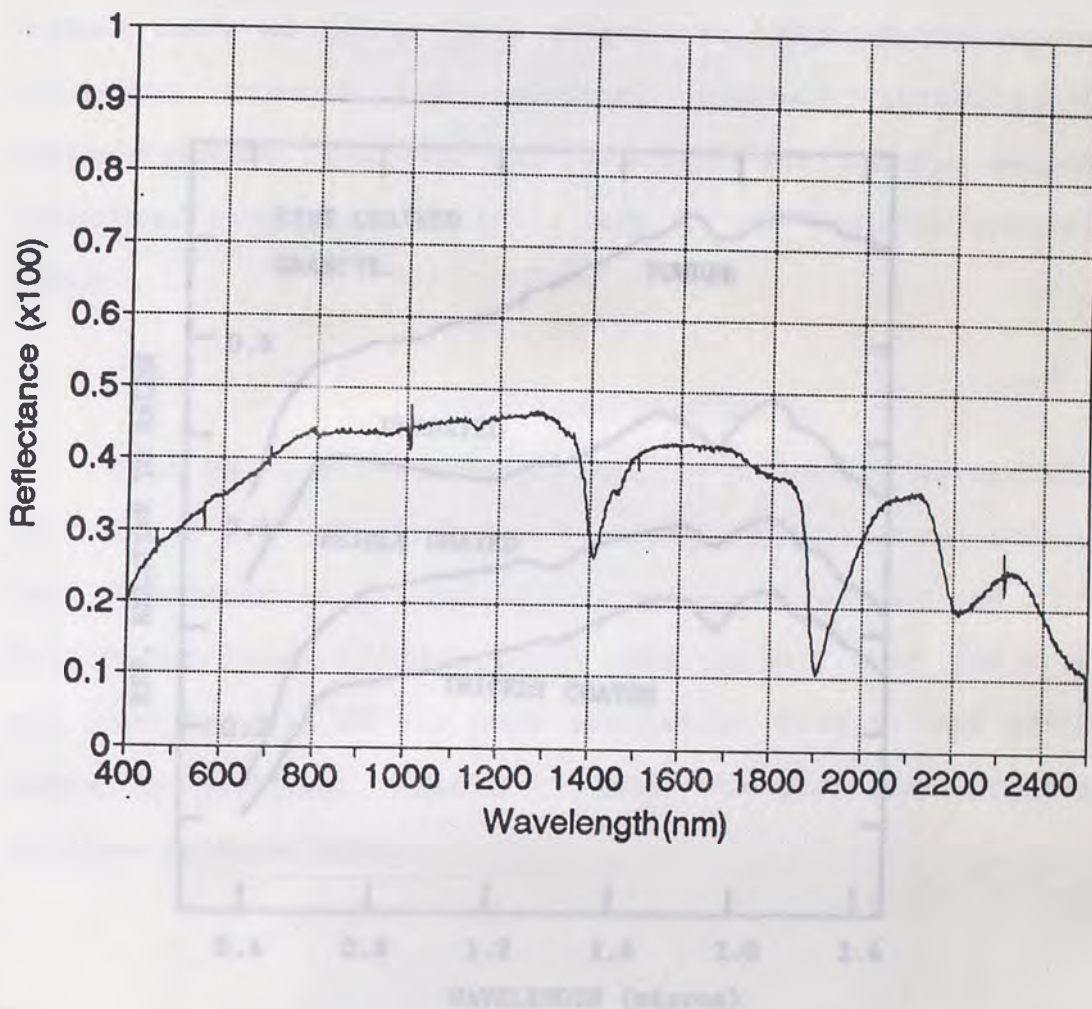


Figure 4-11. Beckman laboratory spectrum of perlite (sample number is 7). Note the clay absorption feature around 2.2  $\mu\text{m}$ .

Ozcan (1972) mapped a granite mass at the northwest of the town Turkali (Figure 2-4). Previously published spectra of granite are shown in Figure 4-12, and exhibit high spectral values in TM bands 5 and 7. These would appear as bright areas in single band images of TM 5 and 7 (Figure 5-1e and f).

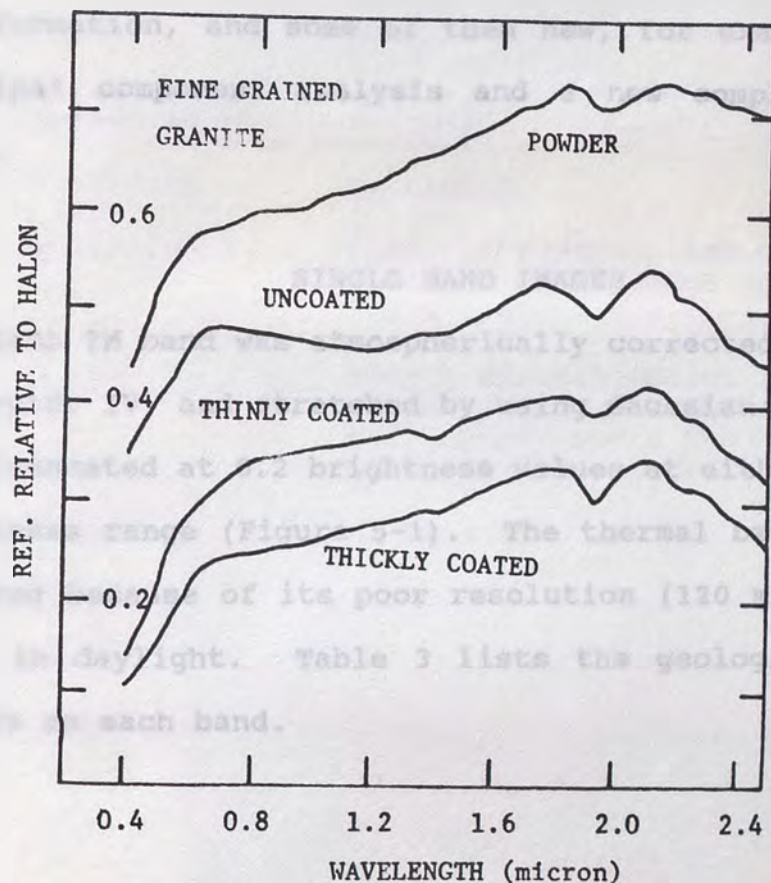


Figure 4-12. Published laboratory spectra of granite (from Sultan et al., 1987).

## CHAPTER V

### IMAGERY ANALYSIS AND RESULTS

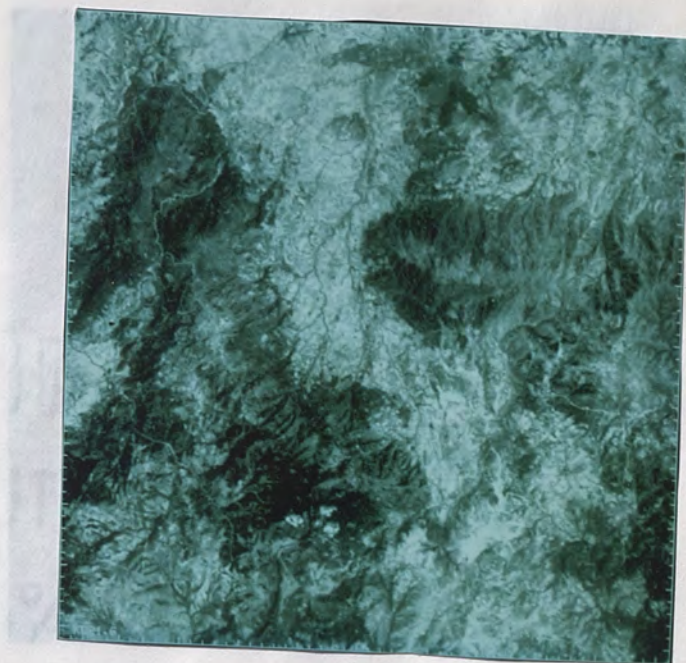
In this section several different image analysis techniques are studied, in order to understand which technique and/or techniques are the most suitable for lithology and alteration discrimination. Some of these methods are conventional such as ratio band composites, principal component analysis, decorrelation stretch, intensity-saturation-hue transformation, and some of them new, for example selected principal component analysis and a new complex composite image.

#### SINGLE BAND IMAGES

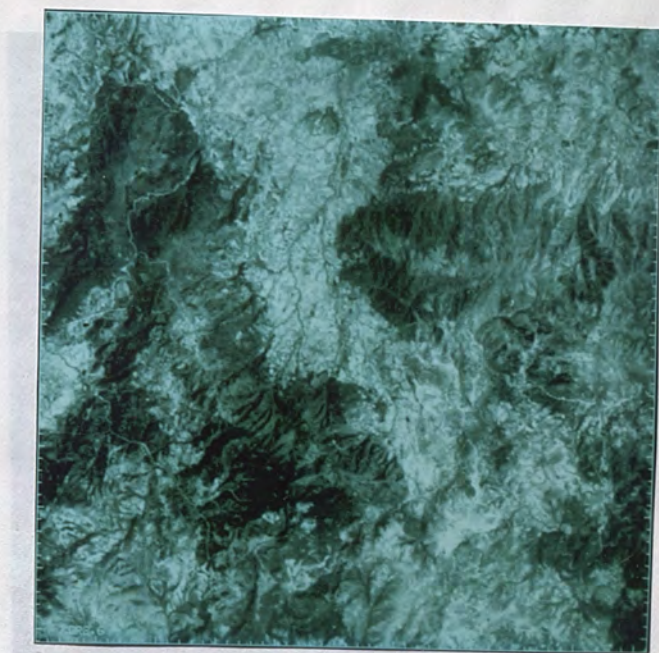
Each TM band was atmospherically corrected as described in chapter IV, and stretched by using Gaussian type stretching, truncated at 0.2 brightness values at either end of the brightness range (Figure 5-1). The thermal band (TM 6) was not used because of its poor resolution (120 m) and performance in daylight. Table 3 lists the geological features visible on each band.

**Table 3.** Geological features discriminated in Thematic Mapper bands 1, 2, 3, 4, 5, and 7.

<u>Band</u>	<u>Wavelength(<math>\mu\text{m}</math>)</u>	<u>Geological Features</u>
1	0.45-0.52	Discriminates the Kinik Formation (dark tones) from sedimentary and volcanic rocks (light tones). Vegetated areas are dark. Alteration is not distinguishable. Roads and river streams are distinguishable.
2	0.52-0.60	As band 1.
3	0.63-0.69	As band 1.
4	0.76-0.90	Shows topography, and structural features. Vegetation appears in light tones
5	1.55-1.75	Better discrimination between metamorphics, volcanics and sedimentary rocks than band 1. Shows structural features.
7	2.08-2.35	As band 5.



(a)



(b)

Figure 5-1. (continued) Atmospherically corrected and stretched TM band 1 (a) and band 2 (b).



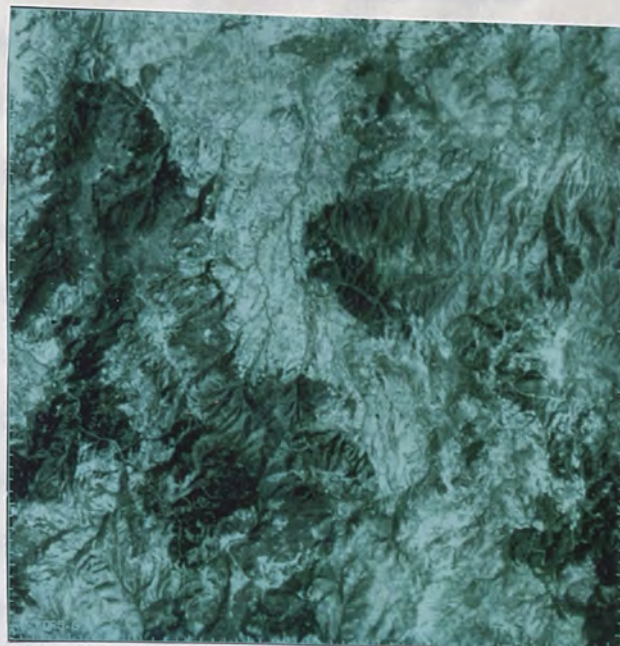
(c)



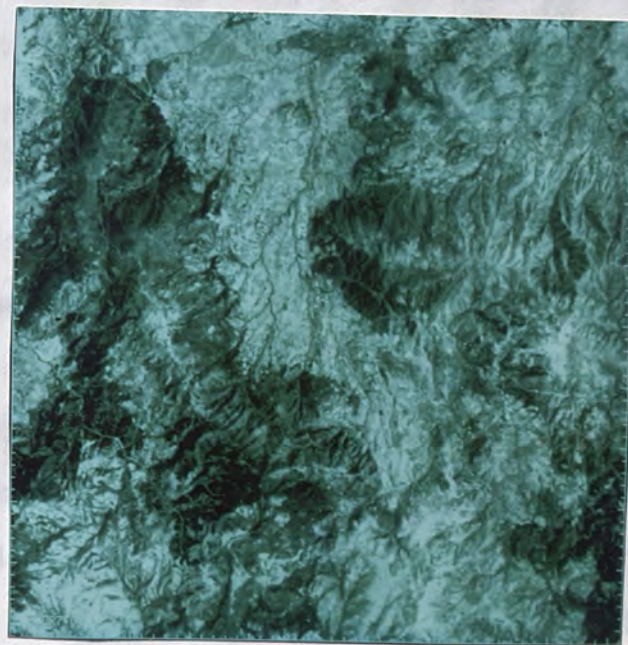
(d)

**Figure 5-1.** (continued) Atmospherically corrected and stretched (Gaussian type) TM band 3 (c) and band 4 (d).





(e)



(f)

**Figure 5-1.** (continued) Atmospherically corrected and stretched (Gaussian type) TM band 5 (e) and band 7 (f).

## SINGLE BAND COMPOSITES

TM bands 4 and 7 cover the most important absorption features of iron and hydrothermally altered minerals respectively (Drury and Hunt, 1988). The calculation of the correlation matrix of the TM bands, excluding the thermal infrared band 6, allows the discrimination of the least correlated bands. In combination with bands 4 and 7, bands 1 and 5 show the "lowest" rank (Feri & Jutz, 1989; Crippen, 1989). The selection of the 4 bands 1,4,5,7 out of 7 reduces the possible 210 RGB permutations to 24. Keeping this fact in mind and after visual inspection of a number of single band color composite images, I chose band combination TM 5,4,1 (in RGB) which shows the greatest spectral difference (Mouat et al., 1986). The TM 5,4,1 single band combination is shown in Figure 5.2. Vegetation and the Kinik Formation (metasandstone, metamudstone, metavolcanics) are displayed in dark green hues due to their spectral similarity in these bands. Vegetation shows very good correspondence with the Kinik Formation's boundaries. A subunit of the Kinik Formation, matasandstones, shows up in dark purple similar to Caldag limestone (4H,4I,4J,5H,5I, Figure 5-2). In the southeast section of the image, andesitic to dacitic volcanics can be distinguishable due to their blue hues. Another area, mapped as granite by Ozcan (1972), appears yellowish (6J, Figure 5-3). The yellow color is a result of high DNs in bands 5 (red) and 4 (green) for granite. This confirms that the granite was correctly mapped by Ozcan (1972).

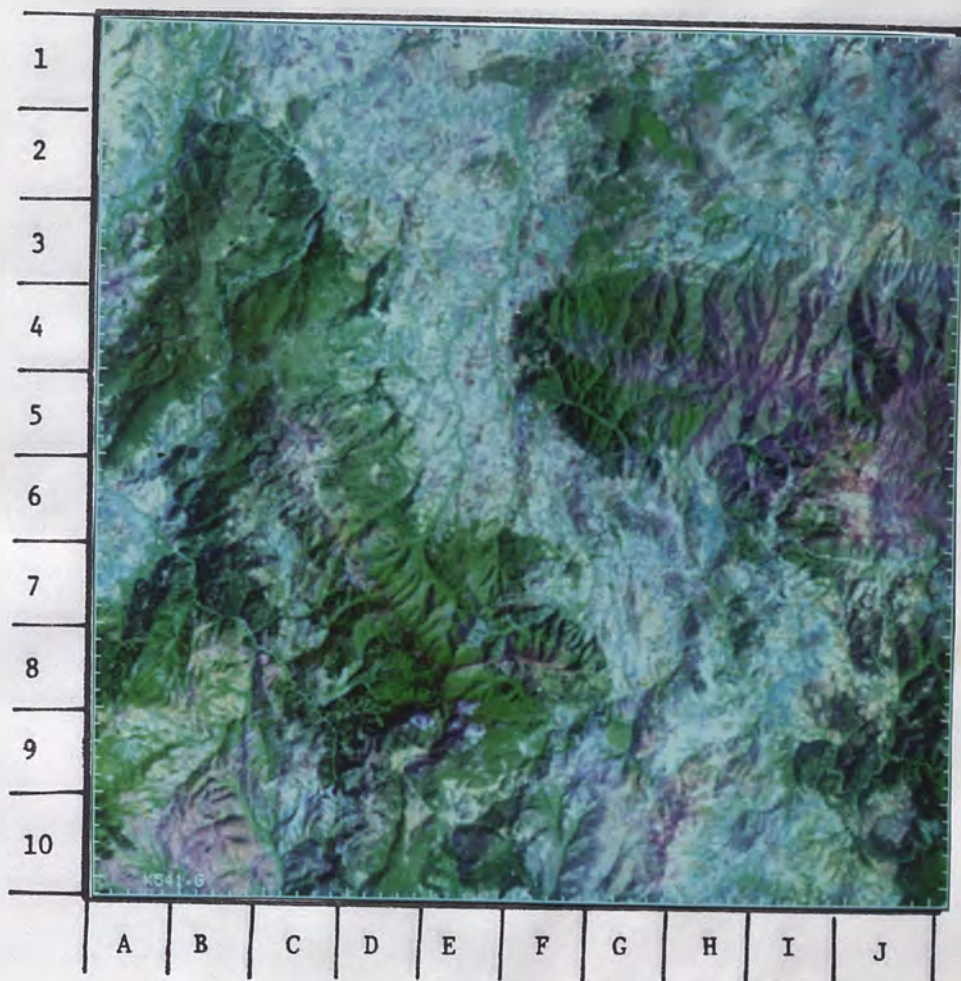


**Figure 5-2.** TM band 5, 4, and 1 (in RGB) composite of the study area (512 x 512 pixels) image. Note distinctive purple over the Kinik and the Caldag Formations due to their relatively high reflectance spectra in band 5 and 1.

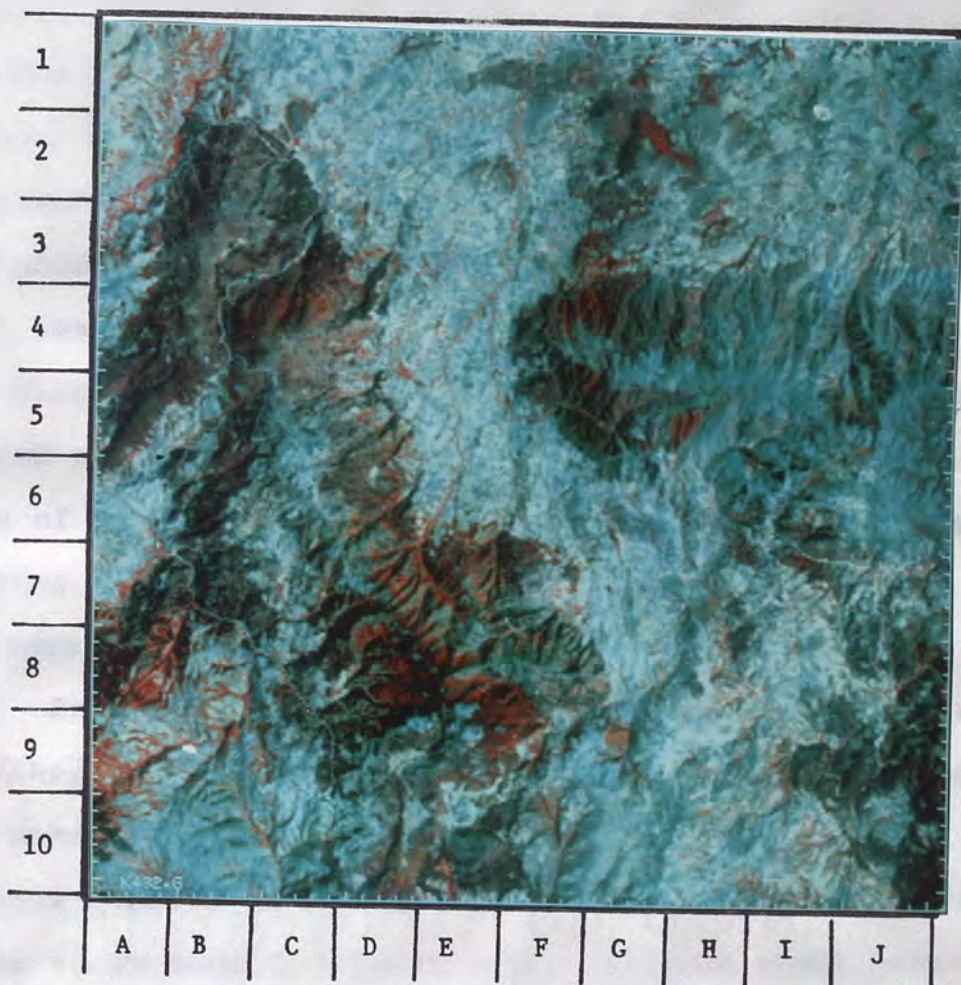


**Figure 5-3.** TM bands 4, 3, and 2 false color image. Note the red hues over vegetated areas due to their high reflectance in band 4 relative to bands 3 and 2.

The TM 4,3,2 composite clearly distinguishes vegetation (Figure 5-3). Vegetation appears in red hues and can be readily distinguished from the Kinik Formation.

#### RATIOS

Band ratioing is a powerful technique for extracting spectral information from multispectral imagery, and is widely used for lithologic and alteration mapping. Band ratio images enhance spectral differences between rocks and suppress topographic effects. As explained in Chapter IV, atmospheric corrections should be made carefully to provide meaningful ratio images.

Multispectral remote sensing is useful for recognizing altered rocks because their reflectance spectra differ from those of the country rock (Sabins, 1987). Many rock units, Yunutdag volcanics, andesites and the Kinik Formation, have been partly hydrothermally altered (Ozcan, 1972; Ercan et al., 1981; Erler and Larson, 1990). Chapter II discusses hydrothermal alteration.

Absorption caused by kaolinite, montmorillonite and clay minerals results in low reflectance at  $2.2 \mu\text{m}$ , which corresponds to TM band 7 (Figure 4-2). Altered rocks have high reflectance at  $1.6 \mu\text{m}$ , which corresponds to TM band 5. A ratio 5/7 image would have bright signatures for altered rocks because the lower reflectance values of band 7 are in the denominator, which results in higher ratio values of approximately 1.5. The unaltered rocks, however, have nearly equal

reflectance values in band 5 and 7 (Figure 4-8) resulting in a ratio 5/7 of approximately 1.0 (Sabins, 1987).

Alteration minerals and iron oxide minerals have weak reflectance in the blue region (TM band 1) and strong reflectance in the red region (TM band 3) (Figure 4-1). The ratio 3/1 has high values for altered and iron-stained areas, resulting in bright tones on the image. Because iron oxide minerals commonly exist in hydrothermally altered zones, the ratio image 3/1 is widely used to distinguish altered areas together with the ratio image 5/7. The spectra of vegetation also show a decrease in reflectance from bands 5 to 7 (Figure 4-8). Therefore, an image of band ratio 5/7 will emphasize vegetation as well as hydroxyl-bearing minerals. In order to overcome this problem, an additional ratio (4/3) was prepared to have high values for vegetated areas due to high reflectance in the near-infrared that is characteristic of green vegetation. The image used to distinguish alteration is a combination of band ratios 3/1 (red), 4/3 (green), and 5/7 (blue), shown in Figure 5-4. In the image, altered rocks and clay-carbonate rich sediments (Soma Formation) are magenta (a combination of red and blue), and vegetation is cyan (a combination of green and blue) to blue. A known hydrothermally altered area (7I,7J,8I,8J, Figure 5-4) in the Yunutdag Volcanics shows a good correspondence with magenta area on the image. Other magenta areas in the Yunutdag Volcanics (9I,9J, Figure 5-4), and in andesites (3J, Figure 5-4) appear as potential altered areas. The magenta areas over the Soma

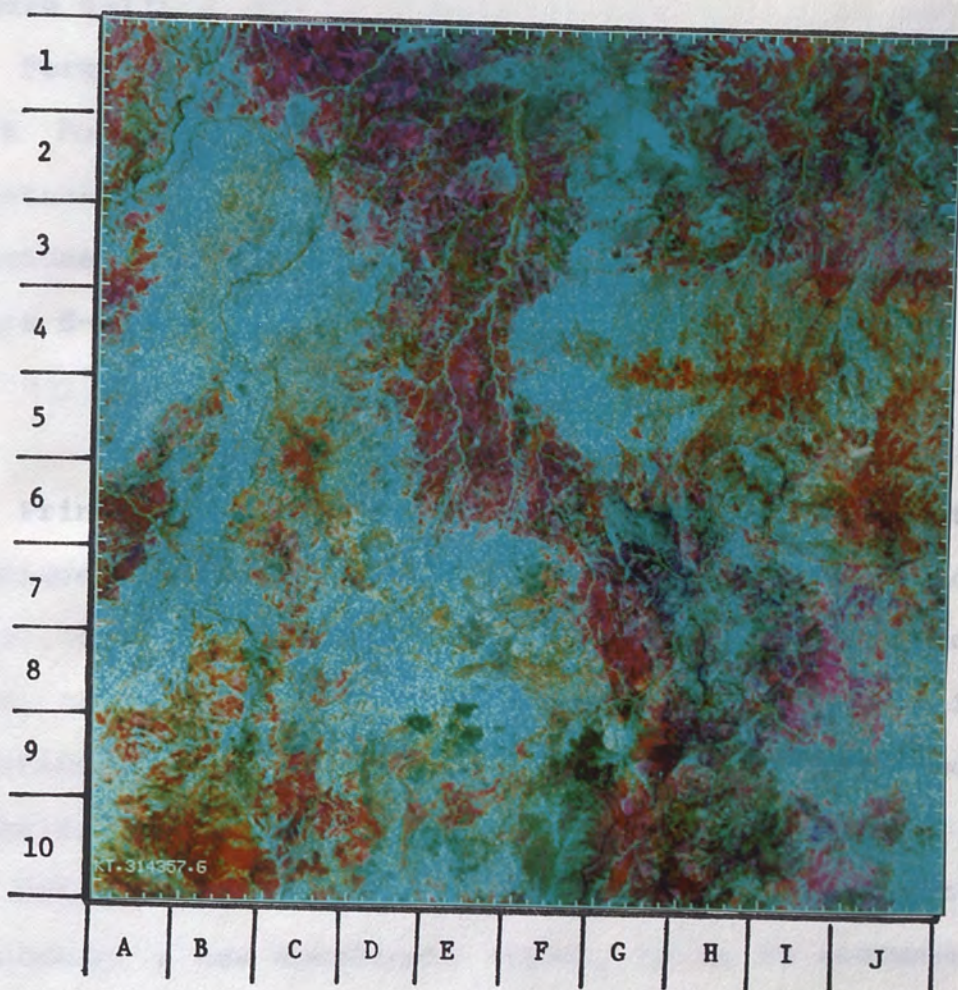


**Figure 5-4.** TM color composite of ratio images 3/1, 4/3 and 5/7 (in RGB). Altered areas in Yunutdag volcanics and andesites appear magenta and are marked by arrows. The magenta areas within the Soma Formation are due to the concentration of clay and carbonate minerals in this formation.

Formation are possibly clay-carbonate rich sediments. These areas need to be checked in the field. Areas of altered volcanic rocks interpreted from this image and selective principal components images (Figure 5-8, Figure 5-9, and Figure 5-10) are outlined in Figure 5-16. Mapped altered areas are associated with a number of linear structures (Figure 5-13).

Permian limestones appear in dark green color on the Kinik Formation (9E,9E,5C, Figure 5-4). Unfortunately, schistose rocks (9A,9B,10A,10B, Figure 5-4), metamorphosed sandstones (5G,5H,5I,5C,6C, Figure 5-4), and granite (6J, Figure 5-4) also appear in a similar red color.

#### PRINCIPAL COMPONENTS ANALYSIS

Principal components analysis (PCA) is a statistical technique occasionally used in remote sensing (e.g., Blodget et al., 1978). Typically, for any pixel in a multispectral image, the brightness values or digital numbers are highly correlated from band to band, so that there is much redundancy in the data set.

PCA is used to compress multichannel image data by calculating a new coordinate system, so as to condense the variance in the original data into a new set of variables which are called principal components (PCs). These data are decorrelated and most of the image variance is confined within the first few channels. After PC transformation, the data are stretched by using nonlinear Gaussian type stretch. This



procedure increases the spectral discrimination capability among terrestrial materials (Qari, 1991).

Visual inspection of the PC color composites indicated that the composite containing the first three PCs was the most informative. This is shown with PC1, PC2, PC3 (in RGB) in Figure 5-5. The Kinik Formation is displayed in dark green hues, due to the vegetation association as explained previously. Heavily vegetated areas appear as a dark blue color in the area. Obvious contacts were detected on the PC color composite image between most of the lithologies, such as the Soma Formation and the Kinik Formation (e.g., 7F, 8G, 9G, Figure 5-5). The dark red areas on the Kinik Formation represent Permian limestone blocks. The Caldag limestone member is shown yellowish green to red color. A slightly metamorphosed sandstone submember of the Kinik Formation appear in greenish yellow (4G, 4H, 4I, 5H, 5I, Figure 5-5). Andesite in the northeast part of the image shows up in cyan to blue color and some andesite blocks are separated in the Yunutdag volcanics (9B, 10B, Figure 5-5).

Another PC composite PC4, PC3, PC2 seemed very useful for discriminating vegetation from the Kinik Formation and to highlight carbonate bearing minerals (Figure 5-6). Vegetation appears in yellow to yellowish green, and the Cavdartepe Formation, Permian limestones and metamorphosed sandstone submember show in hues of magenta. An area (10G, 10G, Figure 5-7) which was not mapped before, appears in magenta and might be a granite or a part of the Cavdartepe Formation according

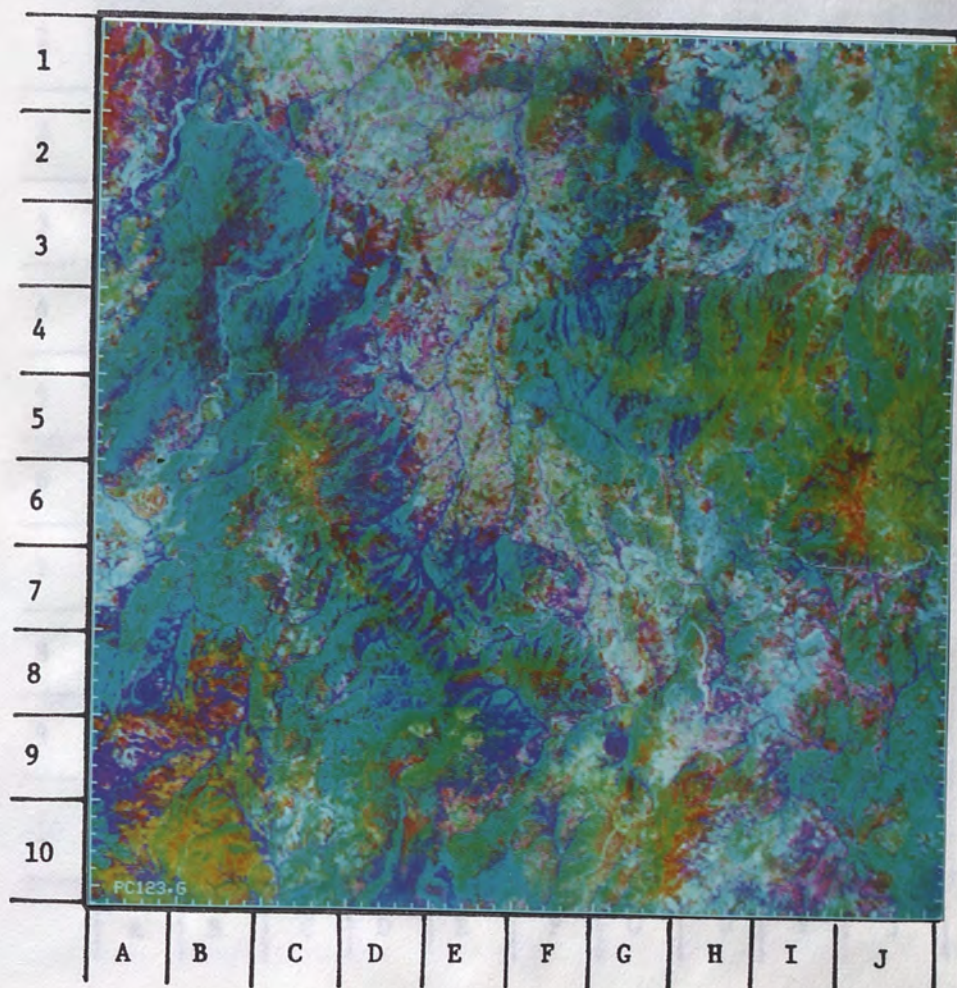
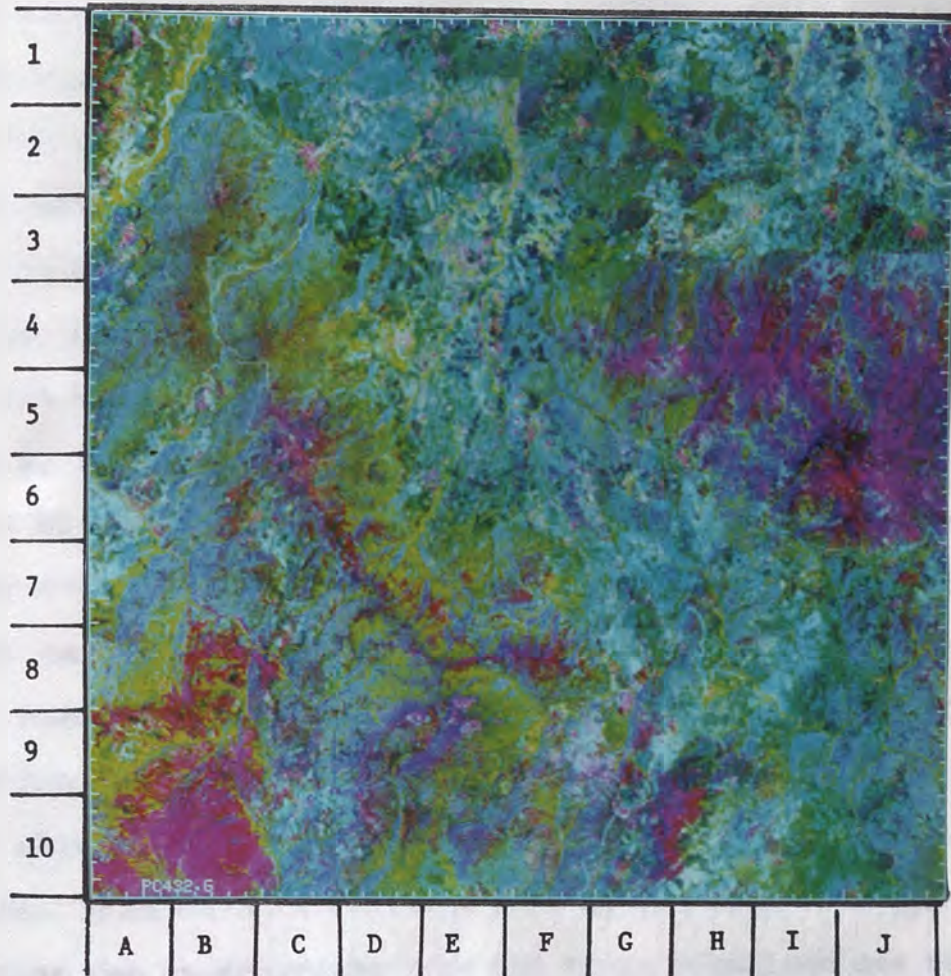


Figure 5-5. Color composite image of principal components PC1, PC2, PC3.



**Figure 5-6.** Color composite of principal components PC4, PC3, and PC2.

to its spectra.

#### DECORRELATION STRETCH

The decorrelation stretch (DS) is another way of emphasizing spectral information in an image. Decorrelation stretching serves to exaggerate color differences which may be subtle in the raw or stretched color composite. Generally, color saturation is increased without significant distortion of the hue (Qari, 1991).

The DS transformation involves using the original eigen vector matrix from the principal components analysis (PCA) in order to create a DS image by transforming that matrix. This results in reordering the PCs back to the domain of the original variables. Most of the information occurs within DS bands 4, 5, 6.

A DS4, DS5 and DS6 color composite (in RGB) is shown in Figure 5-7. In this image most of the lithology boundaries can be easily discriminated. The Soma Formation appears in green hues and the dark magenta color represents the Kinik Formation. The Caldag limestone member has a distinctive blue color which allows easy separation. Vegetation is displayed in pink. The Cavdartepe Formation in the southwest part of the image can be separated from the Kinik Formation due to its darker magenta color. The Rahmanlar Agglomerate unit also can be distinguished from the Soma Formation (7J, 8J, 9G, Figure 5-7) by careful visual inspection at the southeast corner of the area. Altered areas (8K, 8L, 9K, 9L, 10K, Figure 5-7) appear in light green that can be easily distinguishable from

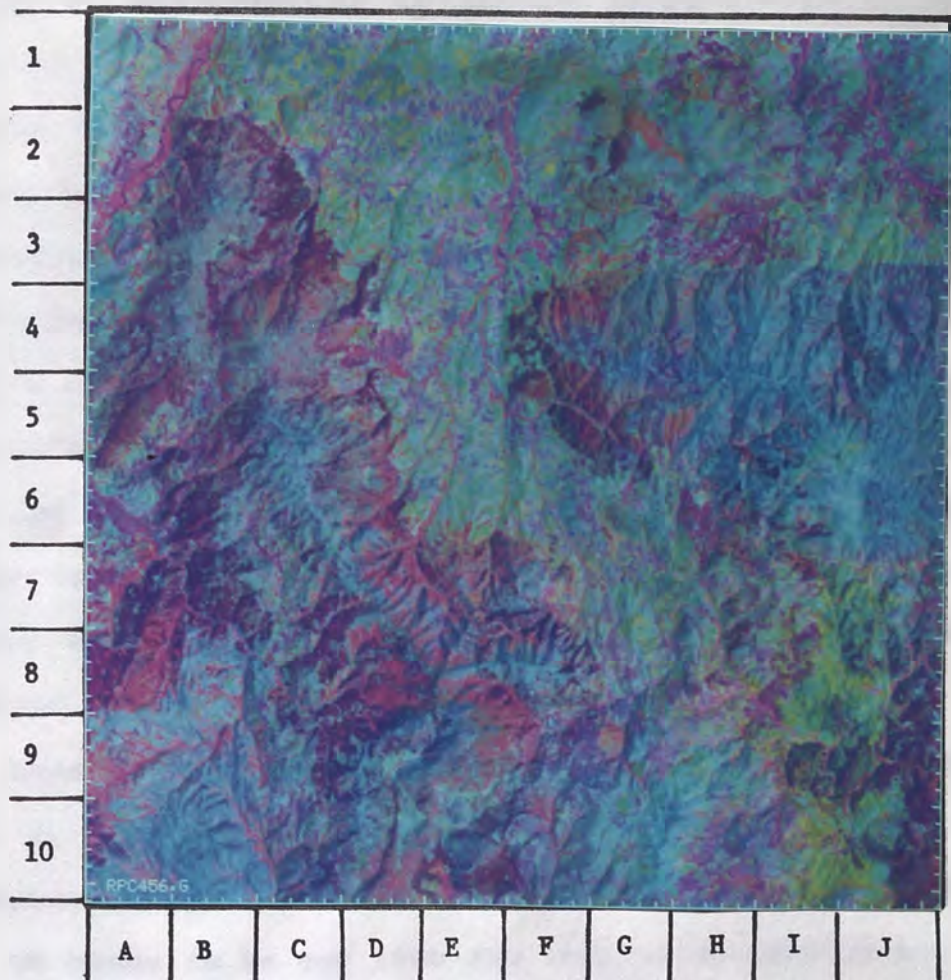


**Figure 5-7.** Color composite image of decorrelation components DS4, DS5, and DS6. Dark magenta and pink represent vegetated areas. Altered areas (3I, 3J, Figure 5-7) are in distinctive light green.

other green hues. Also an area southwest of the village of Cicekli (3I,3J, Figure 5-7) shows up as an altered area where copper mineralization has been reported (Ozcan, 1972).

#### SELECTIVE PRINCIPAL COMPONENT ANALYSIS

A relatively new technique was employed to separate the vegetation contribution in altered areas. The technique known as the Feature Oriented Principal Components Selective (Crosta and McMoore, 1989) is also referred to as the "Crosta technique" or "selective PC analysis". The technique does not necessarily require atmospheric correction, nor even stretching the data (Loughlin, 1991). It is based on the ability of the principal component transform to map increasing subtleties of data variance into successive components. No detailed information is necessary about the spectral properties of specific targets, just a general understanding of the spectral properties of minerals and vegetation is required (Loughlin, 1991).

First, a principal components transformation of TM bands 1, 3, 4, and 5 is made. These TM bands are not stretched and atmospherically corrected. The rationale for choosing these four TM bands is to map iron and iron-oxide bearing minerals in the study area. TM band 7 is especially excluded to avoid contribution of hydroxyl bearing minerals. The magnitude of standard deviations (SD) has the greatest influence over the actual weighting of original bands mapped into PC components. In Table 4 the large SD of TM 5 implies dominance of TM 5 in

PC 1, and the low SD of the vegetation band (TM 4) shows a very low contribution to PC1. Statistics of these bands and the PC transformations were calculated by using ISOCLS and KLTRANS functions of IDIMS software.

**Table 4.** Selected principal component analysis for iron-oxide mapping.

Input Bands	TM1	TM3	TM4	TM5	
Band Means	112.22	66.89	78.60	115.66	
SD of Bands	13.88	18.26	10.75	31.57	
	Eigenvector Matrix				Eigen Values (%)
SPC1	0.3348	0.4509	0.2165	0.7986	93.89
SPC2	0.4851	0.5239	-0.6163	-0.3322	3.41
SPC3	0.3235	0.2758	0.7568	-0.4965	2.37
SPC4	<b>-0.7402</b>	<b>0.6679</b>	<b>0.0248</b>	<b>-0.0784</b>	<b>0.33</b>

Again these bands are stretched. The stretching is done to avoid the influence of the mean and standard deviation of the bands. The stretching is interpreted as a linear transformation of the original data. The stretching is done by using the following formula:

$$Y = \frac{(X - \mu) \cdot \sigma_{new}}{\sigma_{old}} + \mu_{new}$$

where Y is the stretched value, X is the original value,  $\mu$  is the mean, and  $\sigma$  is the standard deviation. Notice the bright color of the iron-oxide band (TM 4) in the iron-oxide image (Figure 2-4). The stretching is done by using the following formula:

**Table 5.** Selected principal component analysis for hydroxyl mapping.

Input Bands	TM1	TM4	TM5	TM7	
Bands Means	112.22	78.60	115.66	56.70	
SD of Bands	13.88	10.75	31.57	19.83	
	Eigenvector Matrix				Eigen Values (%)
SPC1	0.3223	0.2087	0.7847	0.4866	94.67
SPC2	-0.1734	0.9091	0.0611	-0.3737	3.11
SPC3	0.8923	0.1917	-0.4085	-0.0145	1.73
SPC4	<b>-0.2644</b>	<b>0.3052</b>	<b>-0.4622</b>	<b>0.7895</b>	<b>0.49</b>

The SPC1 can be interpreted as albedo. SPC2 describes the contrast between the infrared (IR) and visible (VIS) region (which may be interpreted as vegetation). SPC3 is also brightest for vegetation, and SPC4 high-light iron-oxide bearing minerals as bright pixels (Figure 5-8).

Table 5 describes the PC transformation of a different combination of TM bands 1, 4, 5, and 7 of the study area. Again these bands were not atmospherically corrected and stretched. TM bands 2 and 3 have been especially omitted to avoid the influence of iron oxides. The SPCs can be interpreted as albedo in SPC1, the contrast between near infrared and visible in SPC2, vegetation in SPC3 and hydroxyl-bearing minerals as dark pixels (Loughlin, 1991). This image is negated to show dark pixels as bright areas (Figure 5-9). Notice the bright area (8I, Figure 5-9) which is known to be altered and has a good correlation with the same bright area in the iron-oxide image (Figure 5-8). As mentioned in Chapter



II, this area is hydrothermally altered and has some lead-zinc mineralization (Ozcan, 1972) (Figure 2-4). Another area around the village of Catalan (3I,3J, Figure 5-9) has bright pixels in both images.

This technique is quite successful for alteration mapping in areas having considerable vegetation cover.

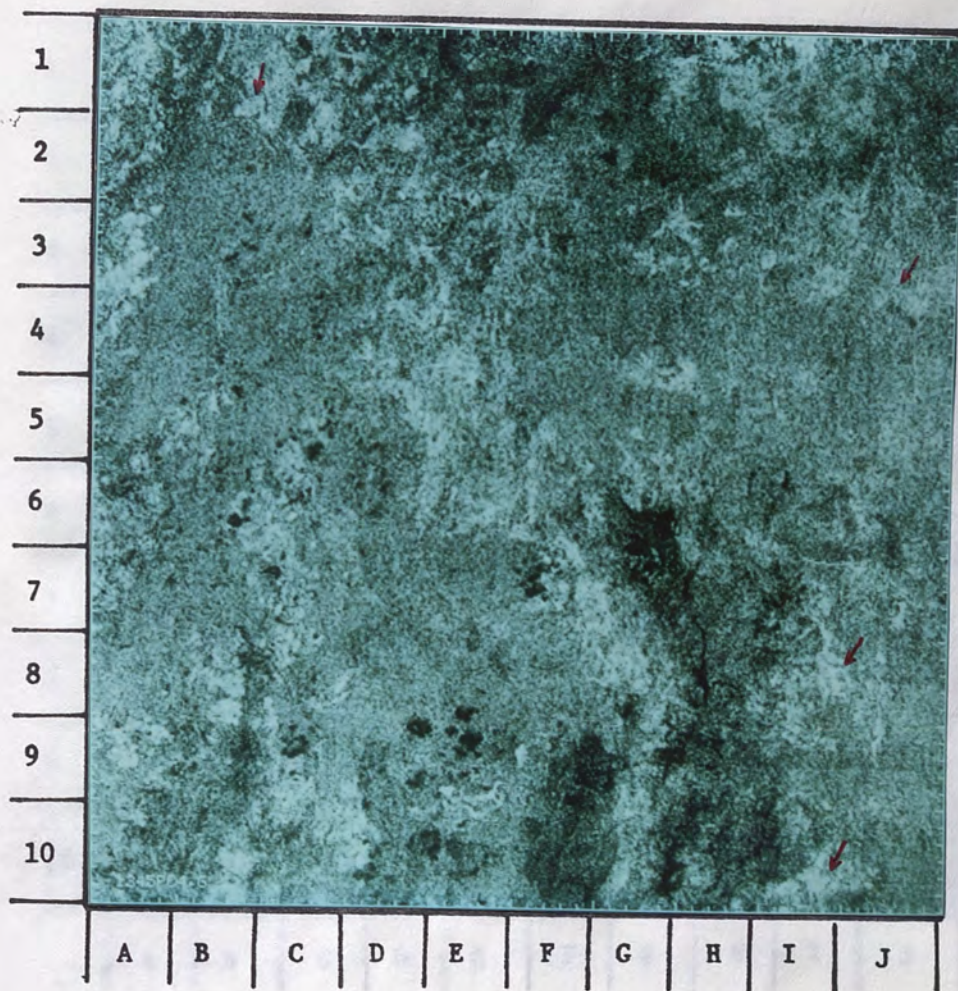
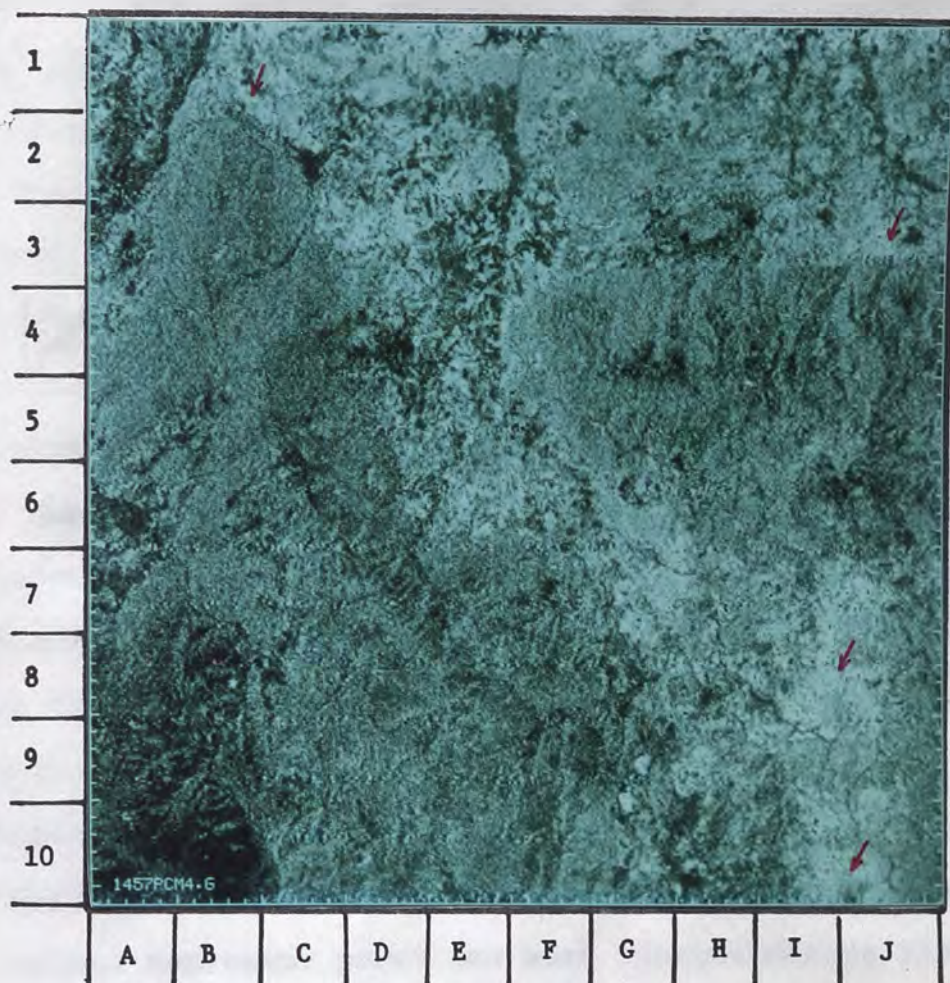


Figure 5-8. SPC4 showing iron-oxide bearing areas as bright pixels. Note the areas indicated by arrows.



**Figure 5-9.** Negated SPC4 of TM bands 1, 4, 5 and 7 which shows hydroxyl bearing areas as bright pixels. Note the areas indicated by arrows.

## ISH TRANSFORMATION

The intensity, saturation, and hue (ISH) transformation has been successfully applied to TM data for cover type discrimination by Borengasser et al. (1984) and Haydn et al. (1982). The ISH system is advantageous because it presents colors as they are perceived by the human observer, i.e. intensity, hue, and saturation are the parameters of human visual perception. They are used to describe color, regardless of the manner in which the color was formed.

The ISH system is based on a color sphere where the vertical axis represents intensity, the radius is saturation, and the circumference is hue. Intensity is a measure of the total light energy reflected from an object, regardless of wavelength (Haydn et al., 1982). Intensity is also a function of albedo (Gillespie et al., 1986). Hue is the average wavelength of light reflected from an object and represents the dominant wavelength of color. Saturation is the width around the average wavelength of the spectral region in which a significant amount of light is reflected from an object. Saturation, therefore, represents the purity of color. Intermediate values of saturation represent pastel shades and high values represent purer and more intense colors (Sabins, 1987).

An ISH transformation image was prepared from TM bands 1, 3, and 5 for the study area (Figure 5-10). The Yunutdag volcanics appear in dark red color which can be discriminated easily from the Soma Formation which appears red and magenta.

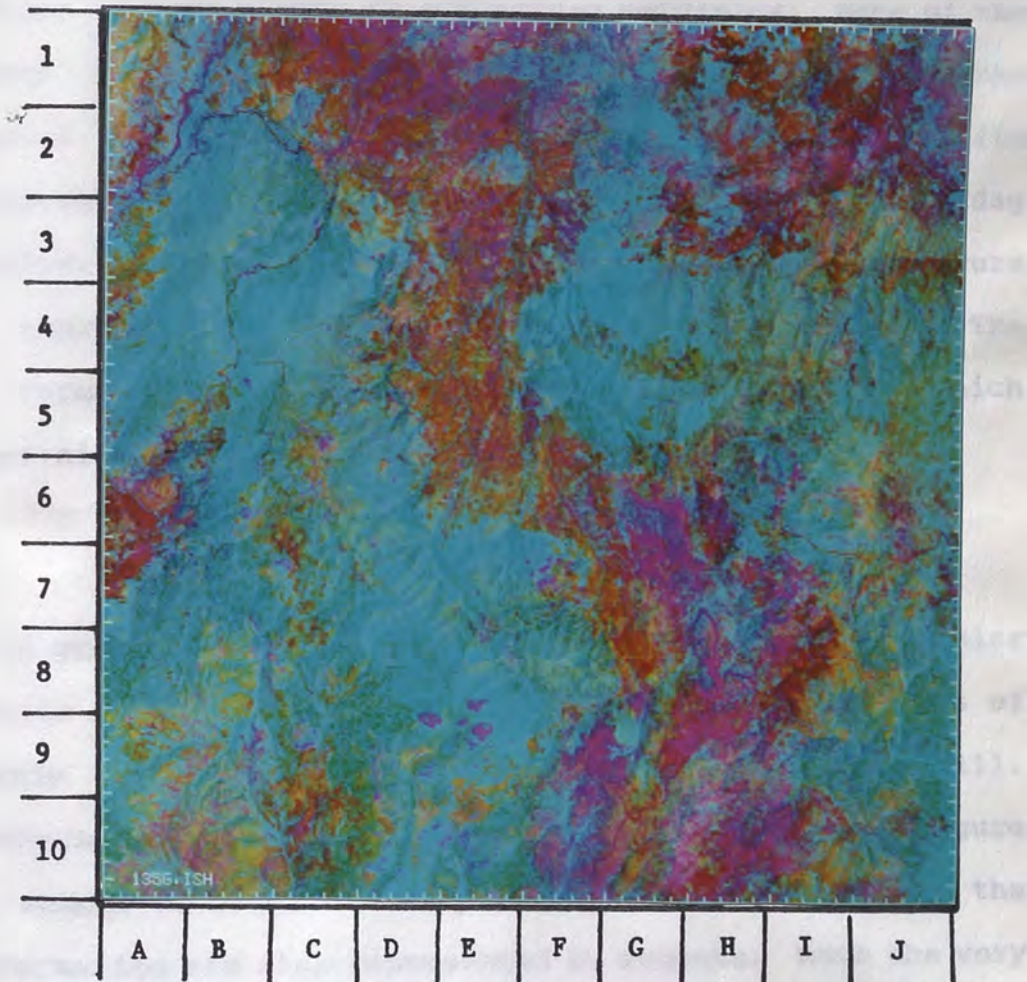


**Figure 5-10.** ISH transformed image of TM bands 1, 3 and 5. Intensity=red, saturation=green, hue=blue. Dacites are in purple hues, andesites are in dark magenta and dark red. Note red areas over the Kinik Formation (7C,10C).

These red areas have a high intensity that corresponds to areas of volcanics and the Soma Formation. Separation of these areas in single band composite images is very difficult, so this ISH composition is quite useful for separating these two units. Note the red areas on the Kinik Formation (7C,9C,10C, Figure 5-10) which might be subunits of the Kinik Formation or some blocks from Yunutdag volcanics. None of the previous techniques were as successful in separating the volcanics as the ISH transformation. The ISH composite distinguished dacite blocks from andesites within the Yunutdag volcanics. Areas in purple hues (6G,7G,8H,9H,9F,10F, Figure 5-10) represent dacites and the Rahmanlar Agglomerate. The Kinik Formation and vegetation shows up in green color which implies high digital values in saturation.

#### COMPLEX COMPOSITE IMAGES

In order to show altered areas more efficiently, a color composite image of SPC4 of TM bands 1,3,4,5, PC4 and SPC4 of TM bands 1,4,5,7, (in RGB) was prepared (Figure 5-11). Hydrothermally altered areas (3J,7I,7J,8I,8J,10I,10J, Figure 5-11) appear as magenta. Clay-carbonate rich areas over the Soma Formation are also represented by magenta. Note the very tiny magenta areas and spots which might be altered areas within the Kinik Formation. Unaltered volcanics are shown in dark green color.

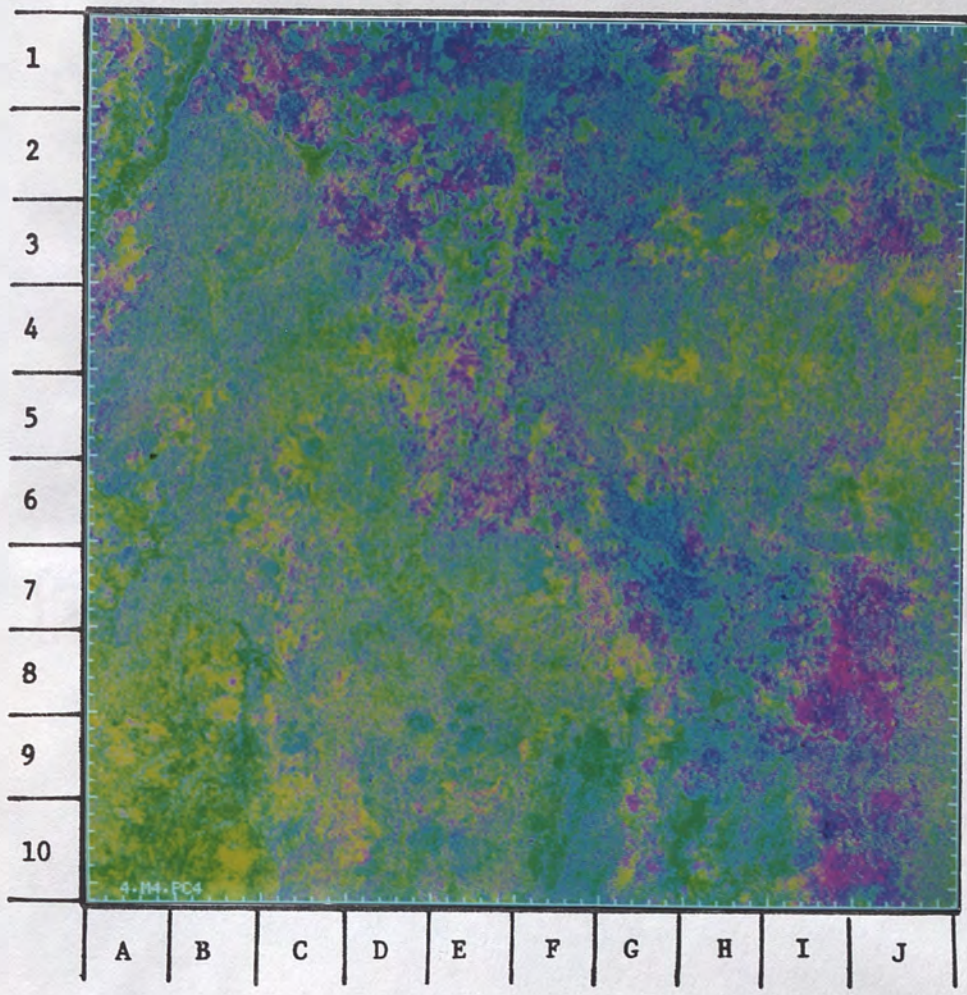


Figure 5-11. Color composite image of SPC4 of TM 1,4,5,7, PC4, and SPC4 of TM 1,3,4,5 (in RGB).

## DIRECTIONAL FILTERING AND STRUCTURAL MAP OF THE AREA

A Laplacian directional filter was used to emphasize higher spatial frequencies. This involved a convolution operation to increase lineament contrast. TM band 5 was selected, and a directional filter was applied. The filter consists of two kernels (Figure 5-12), each of which is an array of three-by-three pixels. The left kernel is multiplied by the  $\cos A$ , where  $A$  is the angle, relative to north, of the linear direction to be enhanced. The right kernel is multiplied by  $\sin A$ . Angles in the northeast quadrant are considered negative; angles in the northwest quadrant are positive. The first time  $A$  was chosen to be  $45^\circ$  and linear features in the northeast direction were highlighted. The second time,  $A$  was chosen to be  $-45^\circ$  to highlight linear features mostly in the northwest. Then  $A$  was assigned  $90^\circ$ ,  $65^\circ$ , and  $-65^\circ$  to highlight lineament in different directions.

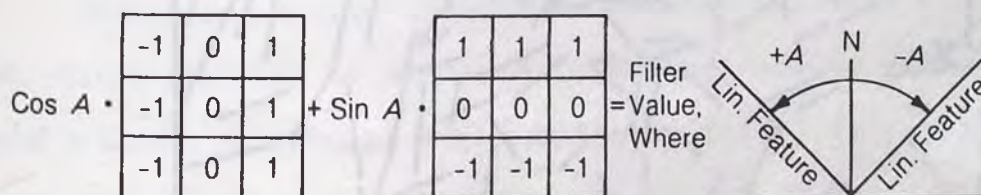


Figure 5-12. Directional filter kernel (from Sabins, 1987).



The lineaments were identified by visual inspection and recorded on a transparent overlay as ruled lines. A remotely sensed lineament map was constructed (Figure 5-13) based on the total knowledge compiled from edge enhancement and single band composites. In addition, known ore mineralizations in the study area were marked on the lineament map (Figure 5-13). They occur along smaller and NNW and E directed faults.

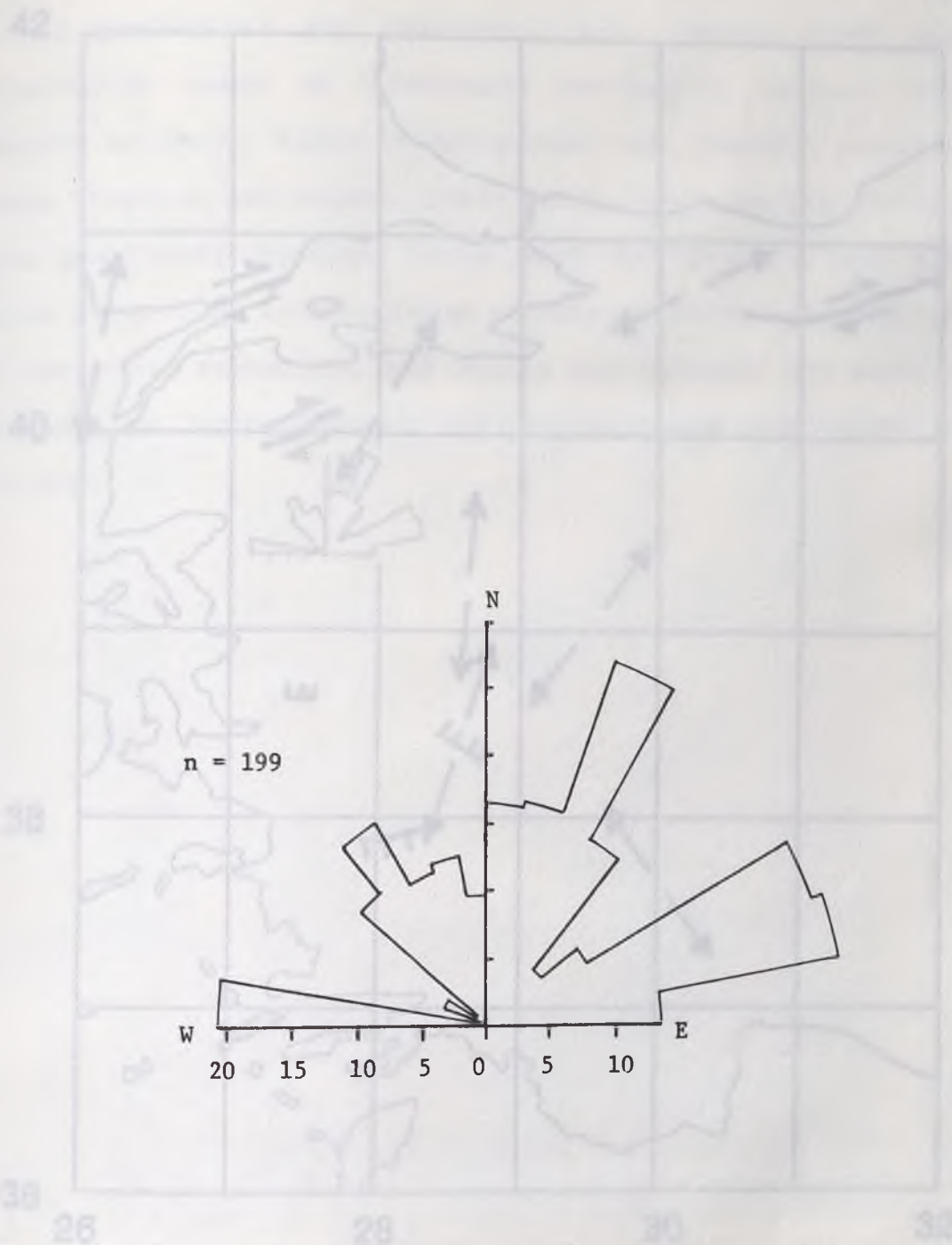


**Figure 5-13.** Lineament map of the study area constructed from directionally filtered images.

Length and trends of lineaments are displayed using a rose diagram in Figure 5-14. The azimuth cell size is 10 degrees, and length is cumulative for all lineaments within each cell. The number of lineaments in the diagram (n) is noted. Lineament trends are strongest at N. 30-40° E., N. 60-80° E., and N 80-90° W. Weaker trends are also concentrated at N. 50-80° W., and N. 40-60° E. The rose diagram of the TM data shows very good correspondence with slip vectors and surface breaks of historical and recent earthquakes in western Turkey (Figure 5-15). This shows that lineament analysis from TM data can aid to map surface features and to explain the tectonics of any area. The use of field observations for lineament analysis is both expensive and, in some cases, inappropriate. TM can be shown to be less expensive and more effective.

The analysis of linear features over western Turkey through the use of TM data may result in valuable information about western Turkey's westward movement and extension direction as well as extension rates.

Fewer and longer lineaments are concentrated at N 30-50° W. while smaller to moderate lineaments are at N 60-80° E., and N 20-30° E (Figure 5-13 and Figure 5-14). In general there are concentrations of lineaments in the NW-SE and WNW-ESE directions. A comparison of plotted lineaments with previously mapped features on the geologic map showed a very good correlation.



Figures 5-13. Slip vectors and surface breaks of historical and recent earthquakes in western Turkey, and the rose diagram of lineaments in the study area. Note the good correlation between the

**Figure 5-14.** Rose diagram of lineaments identified on Landsat TM image in the study area. n = number of lineaments.

42

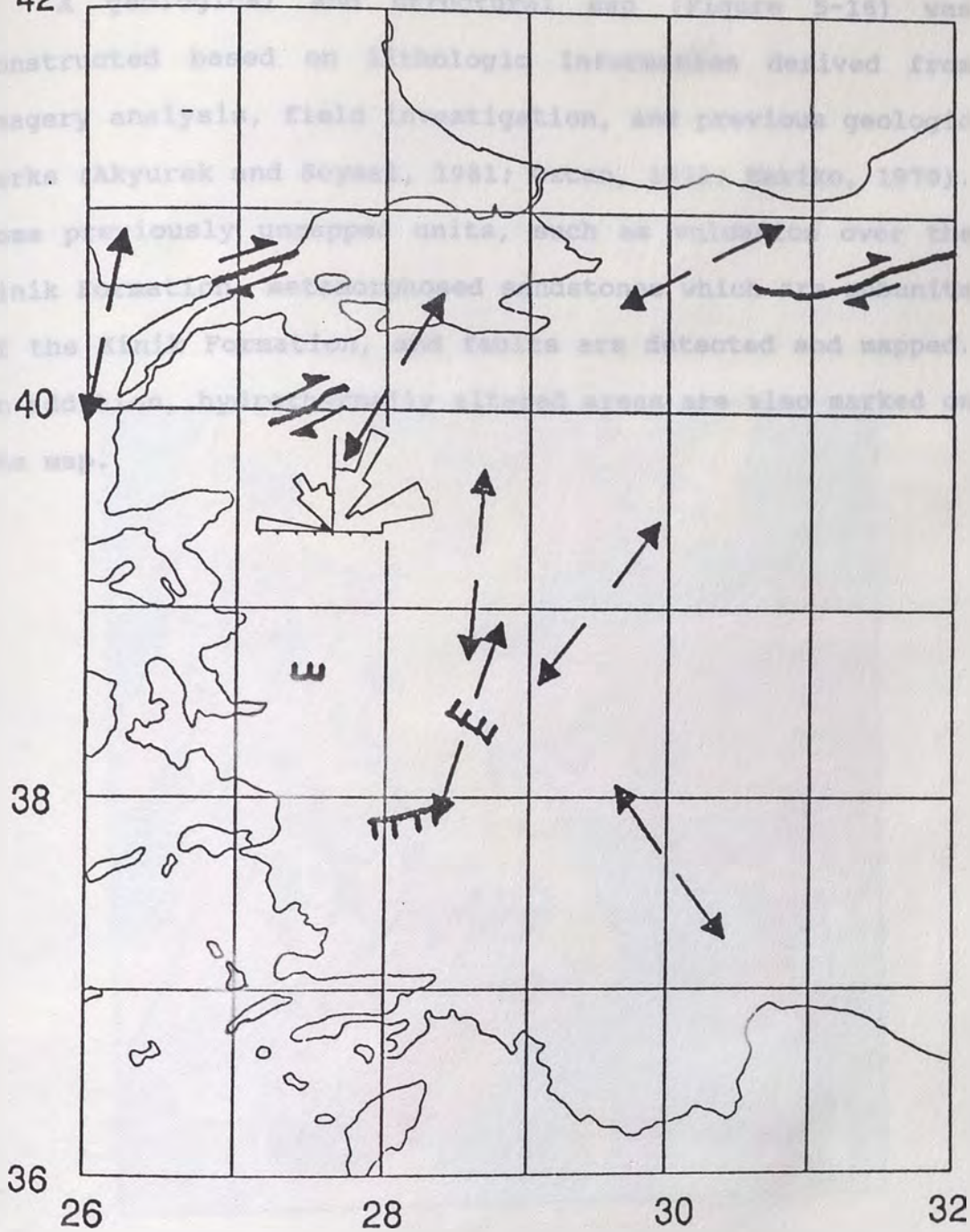


**Figure 5-15.** Slip vectors and surface breaks of historical and recent earthquakes in western Turkey, and the rose diagram of lineaments in the study area. Note the good correlation between the rose diagram and the slip vectors (modified from McKenzie, 1978).

A geological and structural map (Figure 5-16) was constructed based on lithologic information derived from imagery analysis, field investigation, and previous geologic works (Akyurek and Soysal, 1981; Ozcan, 1972; Mariko, 1970). Some previously unmapped units, such as volcanics over the Kinik Formation, metamorphosed sandstones which are subunits of the Kinik Formation, and faults are detected and mapped. In addition, hydrothermally altered areas are also marked on the map.



Figure 5-16. Geological and structural map constructed from the color composites, field work of the author, and works of Akyurek and Soysal (1981), Ozcan (1972), and Mariko (1970).









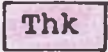


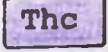






Quaternary		Qa Alluvium
Tertiary		Al Altered areas
		Tr Rahmanlar Agglomerate
		Ts Soma Formation; Lacustrine limestone, marl, sandstone, tuffite
		Tyu Yunutdag Volcanics; Andesite, tuff, silicified tuff, lahar, basalts
		Tyua Andesite
Triassic		Thk Kinik Formation; Metasandstone, metamudstone, metavolcanics
		Thkb Bakirtepe Volcanic Member; Metasplite, metadiabase, metatuff
		Thks Metamorphosed Sandstone
		Thc Cavdarstepe Formation; Green schist
Permian		Pcc Caldag Limestone Member
		Gr Granite
		Fault
		Anticline
		Syncline
		Boundary

Figure 5-16. (continued) Geologic and structural map constructed from the color composites, field work of the author, and works of Akyurek and Soysal (1981), Ozcan (1972), and Mariko (1970).

## CHAPTER VI

### CONCLUSIONS

This chapter emphasizes conclusions drawn from the research and data analysis described in preceding sections. Chapter I includes a list of the major scientific questions addressed by this study, to which the reader is referred. Results of this study support the lithologic discrimination, structural patterns and alteration mapping in Western Turkey.

### GEOLOGIC MAPPING

Lithologic mapping applications of Landsat and other narrow band sensors have not been studied in great detail. The spectral data published by Hunt and Salisbury (1970); Hunt, Salisbury and Lenhoff (1973 a, b, and c, and 1974); Hunt (1977) and Krohn (1985) have had inferential value for Landsat imagery applications. Other researchers have discussed lithologic mapping using Landsat imagery, including Taranik and Trautwein (1977); Abrams and Siegal (1980); Baird (1984); and Davis and others (1987). Sultan and others (1987) contrasted lithologic criteria of some lithologies with TM band DN values and band ratios. Qari (1991) used principal component analysis and decorrelation stretching for lithology discrimination of arid areas.

The best image processing composites have been described in Chapter V; but their useful aspects for lithology mapping will be summarized here:



The PC1,PC2,PC3 (in RGB) composite is very useful for the discrimination of schistose rocks (Cavdarstepe Formation), metasediments-metavolcanics (Kinik Formation), clay and carbonate-rich sediments (Soma Formation) and Tertiary volcanics (Yunutdag Volcanics) from each other. Vegetation is shown with a distinctive dark blue color, and andesites are shown in cyan color that make them readily separable. The granite in the area is located as a red area in this composite image. Most of the boundaries of formations are distinguishable in the study area.

The PC4,PC3,PC2 (in RGB) composite is unique to highlight schistose, metamorphosed sediments, and granites. Unfortunately the composition shows the units in a similar magenta color. Heavily vegetated areas can be easily distinguishable over the Kinik Formation. This composite is very good for lithology discrimination.

The DS4,DS5,DS6 (in RGB) composite is another useful technique that separates vegetation in distinctive dark and light magenta. Formation boundaries are easily separable except the boundary between the Soma Formation and Yunutdag volcanics.

The TM 5.4.1 (in RGB) composite is useful for discriminating sediments, schistose rocks, metasediments and granites. Also most of structural features are distinguishable.

The intensity, saturation, hue (in RGB) composite of TM 1, 3, 5 is the most useful technique to discriminate volcanics

and sediments in the area. Because of similar spectral characteristics of these two units, they are not as easily separable as in other composite images. The volcanics appears as magenta and red with magenta representing dacitic areas, and red representing andesitic areas. These colors make volcanics separable from the sediments which are shown in yellowish red hues. Also this technique made it possible to separate two volcanic areas, which are subunits of the Kinik Formation, over the Kinik Formation.

#### STRUCTURAL FEATURES

#### STRUCTURAL AND MAPPING ALTERED AREAS

Selective principal components analysis and ratio bands color composite gave good results in discriminating the hydrothermally altered areas and potentially altered areas in the study area. The ratio band 5/7 used for hydroxyl-bearing areas, 3/1 for clay and iron-bearing areas, and 4/3 for vegetated areas. The ratio color composite image, 3/1,4/3,5/7 (in RGB) successfully highlighted altered areas having up to 50 percent vegetation cover. The SPC is based on the analysis of eigenvectors which control the content of the PC images, and takes advantage of spectral absorption features caused by hydroxyl-bearing alteration minerals which have relatively low values in TM band 7 compared to TM band 5. Iron-oxide minerals cause relatively low values in TM band 1 and TM band 2 compared to TM band 3. The fourth component of PC transformation (SPC4) of TM 1,3,4,5 bands highlights iron-bearing areas, and the fourth component of the PC

transformation of TM 1,3,5,7 shows hydroxyl-bearing areas as dark. The third component (SPC3) highlights vegetation. Therefore, for areas which have considerable vegetation cover, SPC works very well to separate hydrothermally altered areas.

The applications of both selective principal components analysis and band ratioing helped to discriminate hydrothermally altered areas which occur along lateral and cross faults in the study area.

#### STRUCTURAL FEATURES

Structural analysis was made by using directional high-pass (Laplacian) filtered TM band 5 image, and other color composite images. After eliminating lineaments caused by drainage patterns in the area, a lineament map was constructed. A rose diagram was prepared to observe preferred lineament directions and strike. Known and discovered fault patterns were mapped on a geologic map that had been prepared by using color composite images and previous geologic maps. Topographic effects depicted on color composite images generated in this study, revealed anticlinal and synclinal features. These have been marked on the geologic map. The rose diagram constructed from the TM data showed very good correspondence with previously mapped slip vector and surface breaks of earthquakes in western Turkey. The earthquake surface breaks and slip vectors are used to understand a region's extension direction and extension rate. This lineament information can be extracted from the TM data more

readily than through traditional techniques.

It has been shown that TM image analysis is not only useful in geologic mapping, but also for mapping structural patterns. These structural patterns may not be distinguishable on aerial photographs due to lack of color information which is caused by surface texture, and vegetative cover in these photographs.

As a result of structural analysis, the linear features of the study area have dominant directions at N. 30-40° E. and N. 60-80° E. Known mineralization occurrences are generally located along these NE and E striking faults.

The general conclusions of this study are:

1. TM data is useful for lithologic and alteration mapping in western Turkey.
2. Hydrothermally altered areas can be discriminated in areas having vegetation cover up to 50 %.
3. Lineament information can be extracted from TM data which is important for tectonic and seismological studies.
4. For the purpose of mineral exploration, the use of Landsat TM data may save considerable money and time for locating altered areas and for analyzing structure.

## REFERENCES

- Abrams, M.J. and Siegal, B.S., 1980.** Lithologic Mapping, (Siegal, B.S., and Gillepse, A.R., eds.) Remote Sensing in Geology, John Wiley and Sons, New York, N.Y., pp. 381-418.
- Akyurek, B., and Soysal, Y., 1981.** Basic Geology of the southern Biga Peninsula (Savastepe-Kirkagac-Bergama-Ayvalik) (in Turkish). M.T.A. Periodical, Ankara, 95/96:1-12.
- Ashley, R.P., 1974.** Goldfield Mining District. Nevada Bureau of Mines and Geology Report 19, pp.49-66.
- Baird, A.K., 1984.** Iron Variation Within a Granitic Pluton as Determined by Near-IR Radiometry. Jour. of Geol., 86:344-350.
- Bates, R.L., and Jackson, J.A., 1987.** Glossary of Geology, third edition. McGraw-Hill Book Company, New York, 788 p.
- Bates, R.L., and Jackson, J.A., 1984.** Dictionary of Geological Terms, third edition. Anchor Press, New York, 571 p.
- Blodget, H.W., Gunther, F.J., and Podwysocki, M.H., 1978.** Discrimination of Rock Classes and Alteration Products in Southwestern Saudi Arabia with Computer Enhanced Landsat Data. NASA Technical Paper 1327.
- Borengasser, M.X., Brandshaft, D.R., and Taranik, J.V., 1984.** Geological Application of Enhanced Landsat 4 TM Imagery of South Central Nevada. Proceedings of the Third Thematic Conf. on Remote Sensing for Exploration Geology, Colorado Springs, Colo., 8 p.
- Burkut, Y., 1966.** Kuzeybati Anadoluda Yer Alan Pulutonlarin Mukayeseli Jenetik Etudu. Ph. D. Thesis, Istanbul Technical University Publication, 272 p.
- Collins, A.H., 1988.** Geological Application of Remote Sensing in the Virginia Range, Nevada. Ph. D. Thesis, University of Nevada-Reno, Reno. 241 p.
- Crippen, R.E., 1988.** The Dangers of Underestimating the Importance of Data Adjestments in Band Rationing. Int. J. Remote Sensing, 9(4):767-776.
- Crippen, R.E., 1987.** The Regression Intersection Method of Adjusting Image Data for Band Ratioing. Int. J. Remote Sensing, 8(2):137-155.

- Crippen, R.E.,** 1989. Selection of Landsat TM Band and Band-Ratio Composite Displays. Proceedings of the seventh Thematic Conference on Remote Sensing for Exploration Geology held in Calgary, Canada on 2-6 October 1989, pp. 917-921.
- Crosta, A.P., and Moore, J., McM.,** 1989. Enhancement of Landsat Thematic Mapper Imagery for Residual Soil Mapping in SW Minas Gerais State, Brazil. A Prospecting Case History in Greenstone Belt Terrain. Proceedings of the Seventh Thematic Conference on Remote Sensing for Exploration Geology held in Calgary, Canada on 2-6 October 1989, pp. 1173-1187.
- Davis, P.A., Berlin, G.L. and Chavez, P.S., Jr.,** 1987. Discrimination of Altered Basaltic Rocks in the Southwestern United States by Analysis of Landsat Thematic Mapper Data. Photogrammetric Engineering and Remote Sensing, 53:45-55.
- Drury, S.A., and Hunt, G.A.,** 1988. Remote Sensing of Laterized Archaen Greenstone Terrain. Marshall Pool Area, Northeastern Yildgran Block, Western Australia. Photogrammetric Engineering and Remote Sensing, 54:1717-1725.
- Ercan, T., Gunay, E., and Turkecan, A.,** 1984. Edremit-Korucu Yoresinin (Balikesir) Tersiyer Stratigrafisi Magmatic Kayaclarin Petrolojisi ve Kokensel Yorumu. Bull. of Geol. Soc. of Turkey, 27:21-31.
- Erler, A., and Larson, L.T.,** 1990. Genetic Classification of Gold Occurrences of the Aegean Region of Turkey. Eighteenth Colloquium on Geology of the Aegean Region held in Izmir, Turkey on 2-5 December 1990.
- Frei, M., Jutz, S.L.,** 1989. Use of Thematic Mapper Data for the Detection of Gold Bearing Formations in the Eastern Desert of Egypt. Proceedings of the Seventh Thematic Conference on Remote Sensing for Exploration Geology held in Calgary, Canada on 2-6 October 1989, pp. 1157-1172.
- Gerhard, W.L.,** 1972. Geology and Metasomatic Iron Deposits of the Samli Region, Balikesir Province, Western Turkey. U.S.G.S. Prof. Paper, Paper No 800-D, pp. D75-D87.
- Gillespie, A.L., Kahle, A.B., and Walker R.E.,** 1986. Color Enhancement of Highly Correlated Images. I. Decorrelation and ISH Contrast Stretches. Remote Sensing of Environment, 20:209-235.

- Goetz, A.F.H., 1990.** Concepts and Advancements in Spectral Remote Sensing For Geology. Proceedings of the seventh Thematic Conference on Remote Sensing for Exploration Geology held in Calgary, Canada on 2-6 October 1989, pp. 13.
- Goetz, A.F.H., Vane, G., Solomon, J.E., and Rock, B.N., 1985.** Imaging Spectrometry for Earth Remote Sensing. *Science*, 228:1147-1153.
- Guilbert J.M., and Park, C.F.Jr., 1986.** The Geology of Ore Deposits. W.H. Freeman and Company, New York. 985 p.
- Harvey, R.D., and Vitaliano, C.J., 1964.** Wall-Rock Alteration in the Goldfield District, Nevada. *Journal of Geology*, 72:564-579.
- Haydn, R., Dake, G. W., Henkel, J., and Bare, J.E., 1982.** Application of the ISH Color Transform to the Processing of Multisensor Data and Image Enhancement. IN Proceedings of International Symposium on Remote Sensing of Arid and Semi-Arid Lands, Cairo, Egypt.
- Hunt, G.R., 1979.** Near-Infrared (1.3-2.4 microns) Spectra of Alteration Minerals-Potential For Use in Remote Sensing. *Geophysics*, 44:1974-1986.
- Hunt, G.R., 1977.** Spectral Signatures of Particulate Minerals in the Visible and Near Infrared. *Geophysics*, 42:501-513.
- Hunt, G.R., and Ashley, R.P., 1979.** Spectra of Altered Rocks in the Visible and Near Infrared. *Econ. Geol.*, 74:1613-1629.
- Hunt, G.R., and Salisbury, J.W., 1970.** Visible and Near Infrared Spectra of Minerals and Rocks: Silicate Minerals. *Modern Geol.*, 4:85-106.
- Hunt, G.R., and Salisbury, J.W., 1974.** Mid-Infrared Spectral Behavior of Igneous Rocks. Air Force Cambridge Research Laboratories Report, No: AFCRL-TR-74-0625, 142 p.
- Hunt, G.R., Salisbury, J.W., and Lenhoff, C.J., 1973a.** Visible and Near Infrared Spectra of Minerals and Rocks: VI. Additional Silicates. *Modern Geol.*, 4:85-106.
- Hunt, G.R., Salisbury, J.W., and Lenhoff, C.J., 1973b.** Visible and Near Infrared Spectra of Minerals and Rocks: VII. Acidic igneous Rocks. *Modern Geol.*, 4:217-224.

- Hunt, G.R., Salisbury, J.W., and Lenhoff, C.J., 1973c. Visible and Near Infrared Spectra of Minerals and Rocks: VIII. Intermediate Igneous Rocks. *Modern Geol.*, 4:237-244.
- Hunt, G.R., Salisbury, J.W., and Lenhoff, C.J., 1974. Visible and Near Infrared Spectra of Minerals and Rocks: IX. Basic and Ultrabasic Igneous Rocks. *Modern Geol.*, 5:15-22.
- Izdar, E., 1968. Kozak Intruzif Masifi Petrolojisi ve Paleozoyik Cevre Kayaclarla Jeolojik Bagintilari. *Bull. of Geol. Soc. of Turkey*, 11:140-179.
- Jankovic, S., 1982. Sb-Ag-Tl-Ba Mineral Assemblage of Hydrothermal-Sedimentary Origin, Gumuskoy Deposit, Kutahya, Turkey. IN *Ore Genesis. The State-of-the-Art* (Amstutz, G.C., ed.), pp. 143-149.
- Kaufmann, H., 1988. Mineral Exploration Along the Aqaba-Levant Structure by Use of TM Data Concepts, Processing and Results. *Int. J. Remote Sensing*, 9:1639-1658.
- Krohn, M.D., 1985. Spectral Properties (0.4 to 2.5 microns) of selected rocks associated with disseminated gold and Silver Deposits in Nevada and Idaho. U.S.G.S. Open-File Rep., No 85/576, 23 p.
- Krushensky, R.D., 1976. Neogene Calc-Alkaline Extrusive and Intrusive Rocks of the Karalar Yesiller Area, Northwest Anatolia, Turkey. *Bulletin Volcanologique*, 40:336-360.
- Larson, L.T., 1990. Geology and Gold Mineralization in Western Turkey. *Mining Engineering*, 41:1099-1102.
- Loughlin, W.P., 1991. Principal Component Analysis for Alteration Mapping. *Photogrammetric Engineering & Remote Sensing*, 57:1163-1169.
- Mariko, T., 1970. Geological Map of Yenicekebir (Buyukyenice)-Tasdibi District, Balikesir (in Turkish and English). M.T.A. Open-File Rep., No: 23865, 20 p.
- McKenzie, D., 1978. Active Tectonics of the Alpide-Himalayan Belt. The Aegean Sea and Surrounding Regions. *Geophys. J. R. Astr. Soc.*, 55:217-254.
- Mouat, D.A., Myers, J.S., and Miller N.L., 1986. An Integrated Approach To The Use of Landsat TM Data for Gold Exploration in West Central Nevada. *Proceedings of the Fifth Thematic Conference on Remote Sensing for Exploration Geology* held in Reno, Nevada on 29



- September-2 October, pp. 615-622.
- M.T.A.**, 1970. Arsenic, Mercury, Antimony and Gold Deposits of Turkey, M.T.A. Publication, No: 129, Ankara, 26 p.
- M.T.A.**, 1989. Series of Geologic Map of Turkey, 1:100,000 Scale, Explanatory Text of Balikesir-G4 Quadrangle. M.T.A. Publication, Ankara, 12 p.
- Ongur, T.**, 1972. Dikili-Bergama Jeotermal Arastirma Sahasina Iliskin Jeoloji Raporu. M.T.A. Open-File Rap., No: 5444.
- Ozcan, H.**, 1972. Geologic Map of Cukurlar Area, Ivrindi, Balikesir (in Turkish). M.T.A. Open File-Rep., No: 29165, 12 p.
- Sabins., F.F., Jr.**, 1987. Remote Sensing Principles and Interpretation, W. H. Freeman and Company, New York, 449 p.
- Salisbury, J.W., Walter, L.S., and Vergo, N.**, 1987. Mid-Infrared (2.1-2.5 micron) Spectra of Minerals. First Edition. U.S.G.S. Open-File Rep., No: 87/263, 23 p.
- Sayili, I.S., Gonca, S., and Gevrek, A.I.**, 1990. Gold Mineralization at Arapdag, Karsiyaka, Izmir, Turkey. IN Abst. with Program, of the Int. Earth Scie. Cong. on Aegean Region, Izmir, Turkey, pp. 29-30.
- Sengor, A.M.C.**, 1987. Cross-Faults and Differential Stretching of Hanging Walls in Regions of Low-Angle Normal Faulting. Examples From Western Turkey. IN Coward, M.P., Dewey, J.F., and Hancock, P.L. edit., 1987. Continental Extensional Tectonics. Geol. Soc. of Am., Special Pub., No: 28, pp. 575-589.
- Sengor, A.M.C., Gorur, N., and Sarioglu, F.**, 1985. Strike-Slip Faulting and Related Basin Formation in Zones of Tectonic Escape . Turkey as a Case Study. IN Strike-Slip Deformation Basin Formation and Sedimentation. Soc. of Econ. Paleon. and Min., Spec. Pub., No: 37, pp. 227-246.
- Sultan, M., Arvidson, R.E., Sturchio, N.C., and Guinness, E.A.**, 1987. Lithologic Mapping in Arid Regions with Landsat Thematic Mapper Data, Meatiq Dome, Egypt. Geol. Soc. of Amer. Bull., 99:784-762.
- Spatz, D.M.**, 1989. Genetic, Spectral, and Landsat Thematic Mapper Imagery Relationship Between Desert Varnish and Tertiary Volcanic Host Rocks, Southern Nevada. Ph. D. Thesis, University of Nevada-Reno, Reno. 347 p.

- Taranik, J.V., and Trautwein, C.M., 1977.** Integration of Geological Remote Sensing Techniques in Subsurface Analysis. (LeRoy, ed.) Subsurface Geology. Colorado School of Mines Pub., Golden, Colo., pp. 767-787.
- Qari, M.Y.H.T., 1991.** Application of Landsat TM Data to Geological Studies, Al-Khabt Area, Southern Arabian Shield. Photogrammetric Engineering and Remote Sensing, 57:421-429.

## APPENDIX A

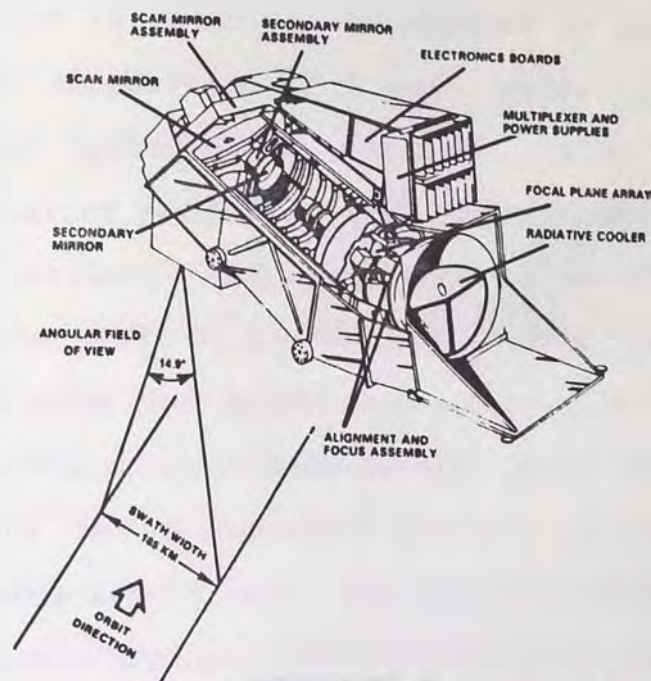
INSTRUMENT AND ORBIT INFORMATION OF LANDSAT 5 THEMATIC

MATTER



Characteristics of Landsat imaging systems

	Multispectral scanner (MSS)	Return-beam vidicon (RBV)	Thematic mapper (TM)
<i>Spectral region</i>			
Visible and reflected IR	0.5 to 1.1 $\mu\text{m}$	0.50 to 0.75 $\mu\text{m}$	0.45 to 2.35 $\mu\text{m}$
Thermal IR (TM band 6)	—	—	10.5 to 12.5 $\mu\text{m}$
Spectral bands	4	1	7
<i>Terrain coverage</i>			
East-west direction	185 km	99 km	185 km
North-south direction	185 km	99 km	170 km
<i>Instantaneous field of view</i>			
Visible and reflected IR	0.087 mrad	0.043 mrad	0.043 mrad
Thermal IR (TM band 6)	—	—	0.17 mrad
<i>Ground resolution cell</i>			
Visible and reflected IR	79 by 79 m	40 by 40 m	30 by 30 m
Thermal IR (TM band 6)	—	—	120 by 120 m
<i>Number of picture elements</i>			
Single band	$7.6 \times 10^6$	$6.1 \times 10^6$	$39 \times 10^6$
All bands	$30.4 \times 10^6$	$6.1 \times 10^6$	$273 \times 10^6$



Thematic-mapper system.

Thematic-mapper spectral bands

Band	Wavelength, $\mu\text{m}$	Characteristics
1	0.45 to 0.52	Blue-green—no MSS equivalent. Maximum penetration of water, which is useful for bathymetric mapping in shallow water. Useful for distinguishing soil from vegetation and deciduous from coniferous plants.
2	0.52 to 0.60	Green—coincident with MSS band 4. Matches green reflectance peak of vegetation, which is useful for assessing plant vigor.
3	0.63 to 0.69	Red—coincident with MSS band 5. Matches a chlorophyll absorption band that is important for discriminating vegetation types.
4	0.76 to 0.90	Reflected IR—coincident with portions of MSS bands 6 and 7. Useful for determining biomass content and for mapping shorelines.
5	1.55 to 1.75	Reflected IR. Indicates moisture content of soil and vegetation. Penetrates thin clouds. Good contrast between vegetation types.
6	10.40 to 12.50	Thermal IR. Nighttime images are useful for thermal mapping and for estimating soil moisture.
7	2.08 to 2.35	Reflected IR. Coincides with an absorption band caused by hydroxyl ions in minerals. Ratios of bands 5 and 7 are potentially useful for mapping hydrothermally altered rocks associated with mineral deposits.

GEOLOGIC ALTERATIONS

Alteration is described as changes in the chemical or mineralogical composition of a rock, generally produced by weathering or hydrothermal solutions (Foster and Jackson, 1947). Weathering results from atmospheric agents at or near the Earth's surface. Most modification occurs at the surface, but it may take place at considerable depths, particularly in well-jointed rocks that permit easy penetration of atmospheric oxygen and circulating surface waters. Many authors restrict weathering to the destructive processes of surface waters occurring below 100 °C and 2 km depth, while the term to include biologic changes and the associated action of wind, water, and ice (Foster and Jackson, 1947).

APPENDIX B

GEOLOGIC ALTERATIONS

Hydrothermal simply means hot water but has been restricted by some to water of volcanic origin. Hydrothermal water includes subsurface water whose temperature is high enough to make it geologically or hydrothermally significant, whether or not it is hotter than the rock containing it. It may include magmatic and metamorphic water, water formed by radioactive decay or energy release associated with faulting, meteoric water that descends slowly enough to acquire the temperature of the rocks it approaches with the normal geothermal gradient but then rises more rapidly so as to retain a distinctly above normal temperature as it approaches the surface, meteoric water that descends to and is heated by cooling intrusive rocks, veins of quartz-saturated granites, and

## GEOLOGIC ALTERATIONS

Alteration is described as changes in the chemical or mineralogical composition of a rock, generally produced by weathering or hydrothermal solutions (Bates and Jackson, 1987). Weathering results from atmospheric agents at or near the Earth's surface. Most weathering occurs at the surface, but it may take place at considerable depths, particularly in well-jointed rocks that permit easy penetration of atmospheric oxygen and circulating surface waters. Some authors restrict weathering to the destructive process of surface waters occurring below 100 °C and 1 kb; others broaden the term to include biologic changes and the corrosive action of wind, water, and ice (Bates and Jackson, 1987).

Hydrothermal simply means hot water but has been restricted by some to water of magmatic origin. Hydrothermal water includes subsurface water whose temperature is high enough to make it geologically or hydrologically significant, whether or not it is hotter than the rock containing it. It may include **magmatic** and metamorphic water, water heated by radioactive decay or energy release associated with faulting, meteoric water that descends slowly enough to acquire the temperature of the rocks in accordance with the normal geothermal gradient but then rises more quickly so as to retain a distinctly above normal temperature as it approaches the surface, meteoric water that descends to and is heated by cooling intrusive rocks, waters of geopressured aquifers, and

brine that accumulates in an area of restricted circulation at the bottom of a sea (Guilbert and Park, 1986).

Hydrothermal action may result in mineral deposition that can constitute a hydrothermal mineral deposit. This involves precipitation of ore and gangue minerals in fractures, faults, breccia openings, or other spaces, by replacement or open-space filling, from hydrothermal fluids ranging in temperature from 50 °C to 700 °C but generally below 400 °C, and ranging in pressure from 1 to 3 kilobars (Bates and Jackson, 1987). Alteration of host rock is common.

Alteration minerals commonly occur in distinct sequences or zones of hydrothermal alteration, relative to the ore body. Not all alteration is associated with ore bodies, and not all ore bodies are marked by alteration zones, but these zones are valuable indicators of possible deposits. Common alteration zones in gold deposits in Nevada (Silberman, 1982; Berger, 1986) are listed below;

- silicic zone
- alunitic zone
- argillic zone
- propylitic zone.

As an example of common hydrothermal alteration zones in vein type gold-silver deposits the Goldfield, Nevada model is shown in Figure B-1. Alteration is most intense where hydrothermal solution entered dacite and andesite country rocks through a fracture, and gold was deposited to form a vein. The



intensity of alteration decreases laterally away from the vein. The following information was summarized from Harvey (1974).

**Silicic zone:** Quartz predominantly replaces the ground mass of host rock immediately adjacent to veins and kaolinite replaces feldspar phenocrysts. Contact with adjacent argillic zones is sharp. All ore deposits occur in veins of the silicic zone, but not all veins contain ore.

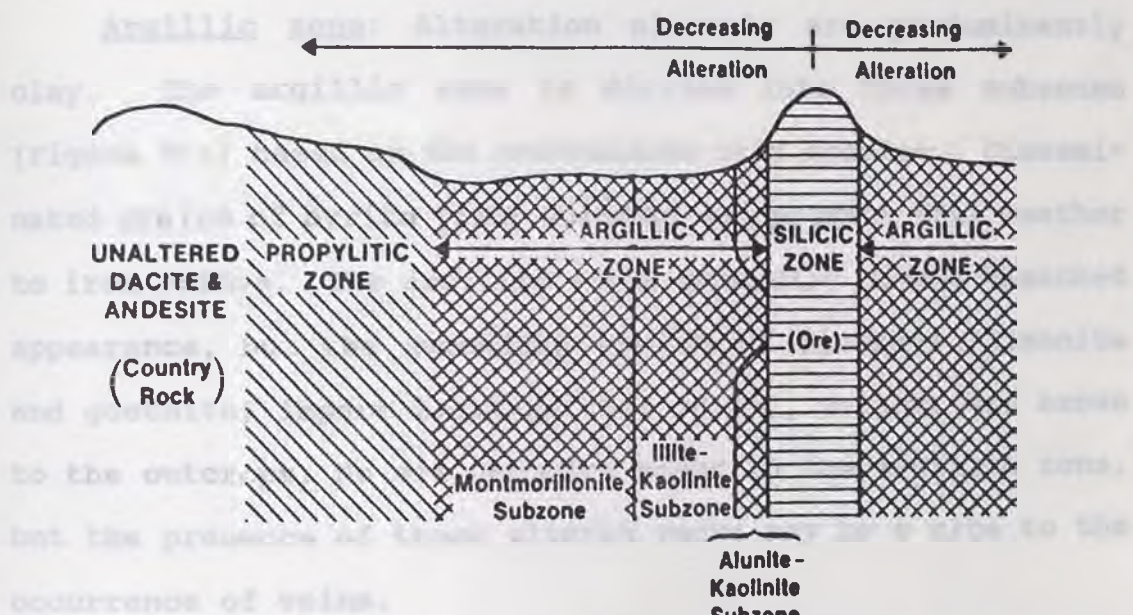


**Figure B-1.** Model cross section of zones of hydrothermal alteration at Goldfield, Nevada. Not to scale. Silicic zone has maximum width of a few meters. Argillic zone is several tens of meters wide (after Ashley, 1974; Harvey and Vitaliano, 1964).

**Montmorillonite subzone:** Montmorillonite is the dominant clay mineral in this subzone, which has a pale yellow color due to jarosite, an iron sulfate mineral.

intensity of alteration decreases laterally away from the vein. The following information are summarized from Ashley (1974). *o. calcite, and antigorite are typical minerals in this*

Silicic zone: Quartz predominantly replaces the ground mass of host rock; subordinate amounts of alunite and kaolinite replace feldspar phenocrysts. Contact with adjacent argillic zones is sharp. All ore deposits occur in veins of the silicic zone, but not all veins contains ore.

Argillic zone: Alteration minerals are predominantly clay. The argillic zone is divided into three subzones (Figure B-1) based on the predominant clay species. Disseminated grains of pyrite (iron sulfide) are present that weather to iron oxides. The argillic rocks generally have a bleached appearance, but the secondary iron oxide minerals (limonite and goethite) impart local patches of red, yellow, and brown to the outcrops. No ore deposits occur in the argillic zone, but the presence of these altered rocks may be a clue to the occurrence of veins.

Alunite-kaolinite subzone: Relatively narrow and locally absent. In addition to alunite and kaolinite, some quartz is present.

Illite-kaolinite subzone: Marked by the occurrence of illite.

Montmorillonite subzone: Montmorillonite is the dominant clay mineral in this subzone, which has a pale yellow color due to jarosite, an iron sulfate mineral.

259

Propylitic zone: These rocks represent regional alteration of lower intensity than the argillic and silicic zones. Chlorite, calcite, and antigorite are typical minerals in this zone. Propylitic alteration is absent at numerous localities in Goldfield, where the argillic zone is in sharp contact with unaltered rocks.

CUSTOMER PROFILE / UNReno Basque Studies  
Profile ID: PUNRbasq

Revised : 09-11-92

28985

ACCOUNT NO: 10262  
ADDRESS: Univ. of Nevada Reno/ Basque Studies  
Dept., Reno, NV. 89507  
CONTACT PERSON: Jane Dixon  
DELIVERY SCHEDULE: 3 Weeks

TELEPHONE NO.: 1-702-784-4578  
BILLING SHEET: LVL  
TRUCK LINE: Willig  
INVOICE

**PRODUCTS**

PERIODICALS: Preservewell  
BOOKS: Preservewell

MEASURE: Flat rate to 14" CALL NUMBERS: No  
MEASURE: Flat rate to 14" CALL NUMBERS: Yes

RECEIVING: Remove the tattle tapes the library places on the verso of leaf 6.

DATA ENTRY / STAMPING: Imprint on spine for periodicals. No imprint for books because location is in the call number. Do not use hyphenated words. Check with library if you have questions about spine information.  
FOIL COLOR: White only TYPE: E and D (18 and 14 point)

DECISION MAKING: Flush to the bottom at bindery discretion for all Nationals and any OS or DFG volumes over 3". Split Nationals over 2" thick into two volumes. All nationals are squareback.

COLLATION: PERIODICALS - Standard collation: Bind everything in. Mending and repair is billable as benchwork. Custom collate only when instructed by library.

BOOKS - Standard collation: Mending of torn pages or guarding of sections is billable as benchwork.

LEAF ATTACHMENT: Periodicals and Books - FIRST choice: Sew Thru Fold, SECOND CHOICE: Double Fan Glue, THIRD choice: Oversew. Pamphlet sew single signatures. Do not saddle sew.

TRIM: Save the Sewing books are NO TRIM. Some titles trim. Many are NO TRIM. Look for specific instructions.

ROUND AND BACK: Preservewell Periodicals that are Double Fan Glued and Oversewed. Do not R&B National sews or Economy Books.

TATTLETAPES: No

BOARDCUTTING: Watch for Flush to the bottoms

PROOFREADING:

INSPECTION & SHIPPING: Bindery slips are to be left in Periodicals and Books.

1-18833